Damage and Deformation of Flexible Electronic Systems

Report of Research Progression Associated with
The Austrian Marshall Plan Foundation Scholarship

By
Colton Katsarelis
March 2017

Advised by
Dr. M. J. Cordill, Department of Materialphysik, Montanuniversität Leoben and Erich
Schmid Institute of Materials Science, Austrian Academy of Sciences
Dr. M. S. Kennedy, Department of Materials Science & Engineering, Clemson University

ABSTRACT

Flexible electronic devices based on thin film technology are being explored and designed for new consumer electronics that can function after repeated stretching and bending. To insure that these devices are capable of withstanding the predicted strains, the electrical and mechanical behavior of the incorporated thin films on flexible substrates must be understood. Some work has already been published in this area, which provided insight on both when mechanical failure occurs in the film and also identified when through thickness cracks initiate and propagate. Other researchers have monitored in-situ resistance measurements to determine when electrical failure occurs in addition to the mechanical failure. Contributions have also detailed how different methods of straining, such as monotonic tensile straining, uniaxial cyclic tensile straining, and bending fatigue, influence the mechanical and electrical reliability.

This study aimed to explore the effects of adhesion layers and substrate on the electro-mechanical performance of Ag films under different loading conditions. The electrical performance (resistance) of Ag film systems during monotonic and cyclic in situ tensile testing. Analysis of the electrical resistance and surface imaging was conducted in an effort to correlate mechanical failures to the electrical behavior. Specifically, we focused on the evolution of cracks within the films as system parameters such as film thickness and adhesion layers were altered. The results showed that the inclusion of an adhesion layer could be detrimental to the electro-mechanical behavior of the Ag films under different loading conditions. It was also observed that the film

thickness also affects the behavior of the films in some ways that appear similar to films with and without adhesion layers. In monotonic tensile testing, the main effects were on the mechanical performance of the films, and in cyclic fatigue testing the effects of adhesion layers and film thickness were observed in both the electrical and mechanical behavior of the Ag films.

ACKNOWLEDGMENTS

acknowledge those at Clemson University who have continued to support this work including Dr. B. Schultz, Ms. G.N. Tomaraei, Ms. C. Johnson, Dr. C. Tonkin, Dr. J. Tong, and Dr. I. Luzinov among many others.

Lastly, I would like to thank my family, immediate and extended, who have supported me from home and abroad throughout my time both at Clemson and during my stay in Austria. Without their love and support, I would not be where I am today.

TABLE OF CONTENTS

LIST OF FIGURES

PAGE

LIST OF TABLES

CHAPTER ONE

Overview of Flexible Electronics Materials, Applications, and Properties

1.1 Introduction to Flexible Electronics

Electronic systems have had a major impact on how people around the world communicate and complete their daily activities. A recent study by Nielsen in 2014 showed that, in the U.S., adults over the age of 18 use electronic devices, such as smartphones, television, computers, and radio, around 11 hours per day on average [1]. The current use and predicted market expansion of electronic devices is driving new materials research in academic, industrial, and government laboratories [2].

While traditional electronic systems utilizing brittle, rigid materials have propelled electronics technology, lightweight, flexible electronics are being explored as options when traditional electronic systems are unable to meet design needs and are being enabled through advancements in thin film technology [2, 3]. Flexible electronics have a diverse range of current and potential applications that include ultra-thin bendable solar cells, foldable displays, conformable sensors, electronic paper, and electronic skin [3–9]. Examples of flexible electronics that are already commercially available (to some extent) include flexible solar cells and electronic paper [3, 8, 10].

Many flexible electronic designs rely on thin film wiring or interconnects between components. These wires or interconnects can be comprised of metallic films deposited onto the flexible substrates. Metals used or explored for use as interconnects include Ag, Al, Au, and Cu. These metals have both relatively high conductivity and ductility. In particular, Ag is known for having the highest conductivity of metals and is currently

being explored for use in printed electronics [4]. An example of printed Ag that could be used as flexible interconnects is shown in Fig. 1.1.
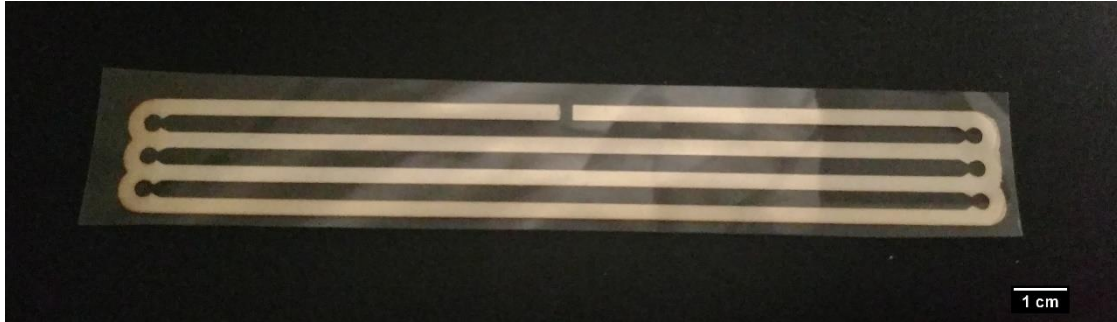
Fig. 1.1: This image shows printed lines deposited with Ag nanoparticle inks and using the flexographic process (CU Sonoco Institute).

In addition to the advantageous physical properties of flexible electronics, the potential for printing of flexible electronics is highly desirable [3–6]. The ability to print flexible electronics could allow for high-throughput production of electronic devices which would make the devices cheaper to produce. Many of these flexible electronic devices are also made with commercial polymers, which if incorporated with printing could allow for cost-effective devices [3, 4].

1.2 Thin Films in Microelectronics

Thin films are commonly considered as films with thicknesses below one micrometer and are often deposited to improve the mechanical, electrical or magnetic performance of a base material or substrate. Not only are thin films found in computers, phones, and automobiles, but also in common appliances such as dishwashers and washing machines, in food packaging and as protective layers for tools and turbine blades. The specific properties of a film are influenced by its microstructure and subsequently, the deposition method.

These deposition techniques can be divided into two main groups, physical vapor deposition (PVD) or chemical vapor deposition (CVD) [11]. The major difference between the two methods is that the CVD process involves chemical reactions to form the film, while with PVD the starting target material has the same composition as the deposited film. Commonly utilized PVD methods include evaporation, sputtering and pulsed laser deposition. CVD techniques include reactive sputtering, electrodeposition, or atomic layer deposition. In both deposition techniques, the processing parameters (pressure, temperature, power and time) will influence the deposited film's microstructure and resulting properties. Just as with bulk materials, the microstructure has a large influence on the properties of the films.

Due to rapid growth of flexible devices and sensors, the assessment and analysis of the interfacial, mechanical and electrical properties of thin films on compliant polymer substrates is increasingly important [5]. Metal and ceramic films have been deposited onto polymer substrates using traditional thin film deposition methods and also with advanced roll-to-roll [12, 13] and inkjet printing [14, 15] techniques. The main advantages of utilizing polymer substrates over the traditional, rigid, ceramic substrates are that polymer substrates are lightweight, flexible (high compliance) and more cost effective. Polymer substrates are much easier and cheaper to produce than single crystalline Si or GaN wafers. Due to the large differences between the elastic moduli of the ceramic, metals, and polymers used to fabricate flexible devices, large strains (>10% and even up to 100%) can be achieved with proper device design [16].

One of the main goals in designing a flexible electronic device is to have a large "stretchability" range. In other words, the flexible device or sensor should be able to stretch and bend without mechanical or electrical failure. A common way to achieve large stretchability is to distribute the rigid thin film transistors over the entire substrate as islands [16–18] and connect the islands with stretchable metal lines. Other ways to improve stretchability include the use of serpentine lines [19, 20], bendable silicon [21], wrinkled conductors [22–24], pre-cracked films or lines [25] or hole geometries [26].

Even though device designs have allowed for greater sustained strains, there is still a need to study the effects of straining on the thin films used as the fundamental underpinnings of the behavior of these film systems is not fully understood. Researchers have examined different methodologies for straining, including uniaxial tensile straining and cyclic bending fatigue [27–33]. The test methods are designed to examine the behavior of the films in straining modes expected during a devices lifetime. This study aimed to explore the behavior of model thin films on polymer substrates under different loading conditions that have been developed by previous studies, and to examine the effects of film thickness and adhesion layers on the electro-mechanical behavior of these model films. In addition, printed metallic films were also studied to compare model films to films with potential use in industry.

CHAPTER TWO

Response of Metallic Films on Polymeric Substrates to Monotonic Tensile Loading

2.1. Introduction

A major concern for flexible electronic design is the capability of the incorporated materials to withstand the strains associated applications while maintaining acceptable electro-mechanical performance. These devices are typically expected to experience mechanical strain during their lifetime by stretching, rolling, bending, or folding, but the materials must also withstand the strains and bending modes that may be associated with the manufacturing process as well as those applied by the end user [5]. Many published studies have reported on the methodology of applying strain to flexible systems [5, 32, 34–36]. As applications of flexible electronics have diversified, the range of techniques to apply have evolved. Two of the most commonly studied straining methods are uniaxial tensile testing or stretching and cyclic bending fatigue testing [32, 34, 29, 37].

Uniaxial tensile testing can be separated into two categories: monotonic and low cycle tensile straining. In monotonic tensile testing, a sample is only loaded and unloaded once. The maximum strain of each test is selected based on the film and substrate couple. The strains tested in metal films can vary greatly with different film parameters demonstrated by Xiang et al. which showed the effects of film adhesion to the substrate by testing strains from 2% to 30% [32]. In contrast, cyclic tensile testing focuses mostly tensile loading where samples are repeatedly loaded to low strains and unloaded for low cycle counts (Cycles ≤ 10,000) [36].

As part of these testing methods, resistance is often monitored since the films are meant for electronics applications. Changes in resistance, as noted in Glushko et al. [37], can be attributed to changes in sample geometry and structural modifications of the film, most notably the formation of necks and cracks. The resistance, R, metallic film or line can be calculated as:

$$R = \rho \frac{L}{A} \qquad (2.1)$$

where ρ is resistivity, L is sample length or gage length in tensile testing, and A is the cross-sectional area. Resistivity is a material property and is therefore assumed to remain constant and the initial resistance can be defined by:

$$R_0 = \rho \frac{L_0}{A_0} \qquad (2.2)$$

Where R_0, L_0, and A_0 represent the initial resistance, gage length, and cross-sectional area, respectively. It should be noted that the resistivity of a film is a function of the microstructure and as the number of grain boundaries, dislocations or other defects increases, the resistivity will also increase. A normalized resistance (R/R_0) can then be formulated using Eq. 1 as the resistance during straining where L is the gage length during straining ($L = L_0 + \Delta L$) and A is the cross-sectional area. In the elastic region, the engineering strain ($\epsilon = \Delta L/L$) and Poisson's ratio, v, is related to the normalized resistance by:

$$\frac{R}{R_0} = (1 + 2v) \cdot \epsilon + 1 \qquad (2.3)$$

where the variables are as defined for prior equations. As a film is plastically deformed, it can be assumed that the volume of the sample is held constant ($L \times A = L_0 \times A_0$) and the

relationship between strain and normalized resistance can be given by Eq. 2.4 and shown in Fig. 2.1.[35, 30]:

$$\frac{R}{R_0} = \left(\frac{L}{L_0}\right)^2 \equiv (1 + \epsilon)^2 \qquad (2.4)$$
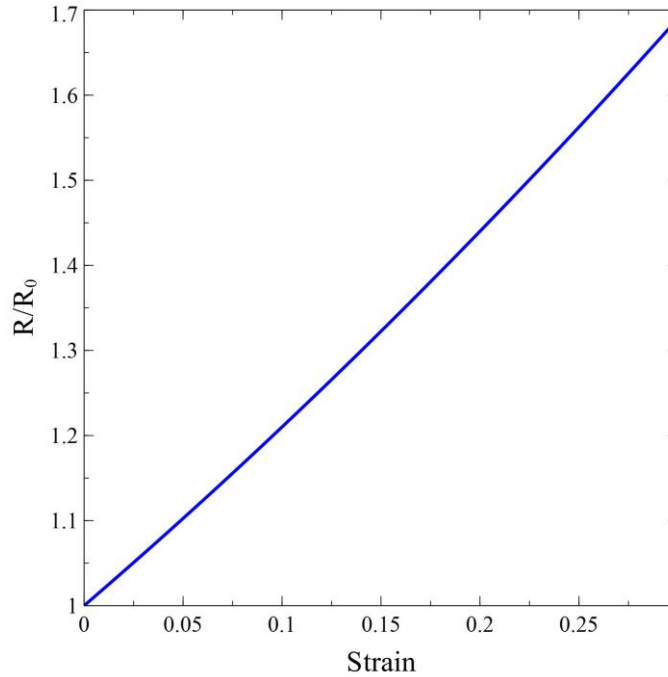
Fig 2.1: The change in resistance of metallic films during tensile strains can be predicted using equation 2.4. This model only takes into account the strain of the system and no other factors, such as the strain hardening coefficient, film thickness, or grain size.

In monotonic tensile testing, resistance is expected to follow the line shown in Fig. 2.1, plotted from Eq. 2.4, until a deviation strain occurs within ductile films or a fracture strain for brittle films is reached. In ductile films, this deviation from the theory most likely indicates a critical density of necking or cracking in the film independent of the substrate has occurred, and if the film continues to be strained after this point, through thickness cracks will propagate further [32, 37]. For brittle films, deviation at the fracture

strain indicates that cracks have started to develop causing increases in resistance. It should be noted that the resistance ratio (R/R$_0$) is only a good indicator for brittle film fracture, due to the fact that when through thickness cracks form they generally form across the whole sample width. As soon as a through thickness crack forms across the entire sample width, the electrical resistance increases because the crack does not allow current to flow. The *R/R$_0$* ratio has been shown to be useful to determine the crack onset strain, or fracture strain, of brittle films such as Mo, printed Ag, or ITO [31, 27, 38]. In ductile films, like Au, Cu, and Ag, plastic deformation occurs before through thickness cracks form. This deformation is dependent on the films thickness and microstructure[39–41]. What is different about the *R/R$_0$* response for ductile films under tension is that the deviation from theory can be a consequence of the formation of necks, or localized regions of the film that are thinning [42], or the formation of a high density of short through thickness cracks [43]. The correlation of the different deformation mechanisms and the electrical resistance in ductile films have not been adequately investigated, thus leading to the reporting of crack onset strains that are not related to actual crack formation [39]. Under cyclic loading, ductile films can have room temperature grain growth, form extrusions followed by through thickness cracks [36], or severely roughen the surface [36]. The type of deformation influences the electrical response and thus the lifetime. Brittle films subjected to cyclic tensile loading will form cracks and the crack length growth can be reflected in the electrical response.

2.2. Experimental Methods

    2.2.1. Deposition of Metallic Films and Characterization

Ag thin films were deposited onto six different substrates using sputter deposition. The substrates included 125 μm polyimide sheet (DuPont Kapton HN), 127 μm polyimide roll (DuPont Kapton HN), 100 μm polyethylene naphthalate (PEN) (DuPont Teijin Teonex), 100 μm polyethylene terephthalate (PET) (Mitsubishi Hostaphan RN), 130 μm polytetrafluoroethylene (PTFE) (DuPont Teflon FEP), and Si wafers. Films were deposited with thicknesses of 900 nm, with and without a 45 nm Ti adhesion layer, for all substrates and 1.8 μm for the polyimide sheet, PEN, and Si wafer. Substrates were sectioned into dimensions 70 mm by 297 mm. Deposition was performed using a Kurt J. Lesker sputter deposition system using the parameters in Table 2.1 at Clemson University. Film systems fabricated for this study were designed to observe the impact of film and substrate properties, presence of adhesion interlayers, and film thickness.

Table 2.1: Deposition parameters for Ag and Ti films deposited in this study.

Film Material	Ag	Ti
Target Purity	99.9 %	99.9 %
Base Pressure	1.8×10^{-6} Torr	1.8×10^{-6} Torr
Working Pressure (Ar)	9.5×10^{-3} Torr	9.5×10^{-3} Torr
Power	200 W RF	100 W DC
Sputter Rate	12.6 nm/min	4.5 nm/min

In addition to PVD films, 1.25 μm thick flexographic printed Ag lines were provided by the Clemson University's Sonoco Institute of Packaging Design and Graphics. This sample set allowed for direct comparison between model films to films

with application in industry. The films were printed using an OMET Varylex 530 system with PChem PFI-722 silver nanoparticle ink onto a DuPont Teijin Heat Stable substrate. Further details of the printing process can be found in [44].

Optical microscopy (Zeiss BX-51) and scanning electron microscope (SEM, a Zeiss Leo 1525) were used to examine the surfaces of both the as-deposited films and characterize the films after mechanical testing to characterize the defects, cracks, and buckles that may have been formed.

2.2.2. Monotonic Tensile Testing

The response to monotonic tensile strain was performed using a MTS Tytron 250 with a four-point probe set-up incorporated into the sample grips to measure changes in resistance across the film in-situ with a Keithley 2000 multimeter. More information on the set up can be found in [37]. Samples for testing were sectioned to dimensions 5 mm by 35 mm with a gauge length of 15 mm. Tensile tests were performed at a velocity of 5 μm/s to a maximum strain of 30%. Samples tested using these methods are indicated in Table 2.2.

Table 2.2: Film systems fabricated for this study were designed to observe the impact of film and substrate properties, presence of an adhesion interlayer (Ti), and film thickness.

Film	900 nm Ag	900 nm Ag/Ti	1.8 μm Ag
Substrate			
PI Sheet	x	x	x
PI Roll	x	x	
PET	x	x	
PEN	x	x	
PTFE	x	x	
	1.25 μm Printed Ag		
PET	x		

2.3. Results and Discussion

2.3.1. Ag/Kapton Films

The change in normalized resistance during monotonic tensile loading for 900 nm Ag film systems on Kapton is shown in Fig. 2.2 ((a) Ag/Kapton and (b) Ag/Ti/Kapton). The loading and unloading curves for the Ag films with and without Ti interlayers are compared with the theory line given by Eq. 2.4. Both of these curves show the expected behavior of normalized resistance increasing upon loading, decreasing upon unloading, and after unloading the magnitude of normalized resistance is larger than the initial value.

The normalized resistance of the Ag/Kapton (a) and Ag/Ti/Kapton (b) systems were observed to have fallen below or followed the theory up to 30% strain. The behavior of the Ag/Kapton system was unexpected as the normalized resistance was expected to follow the theory line or deviate above it, but if Eq. 2.3 is used with $v = 0.34$ for Kapton, the normalized resistance curve for the Ag/Kapton curve follows this line. This behavior of the Ag/Kapton curve to fall below the general theory line is not fully understood and could be a consequence of the initial film microstructure or of the four-point-probe technique itself. Others have also observed behavior that drops below the theory line, such as in Al on PI [45] or Cu on PI [46]. A more intense investigation is necessary before strong conclusions can be drawn. However, there could be a region of the normalized resistance-strain plots in which the normalized resistance curves may fall, and the positioning of this region could be affected by variables that are neglected by Eq. 2.4 due to assumptions. The electro-mechanical behavior of the film has also been shown to be affected by the film thickness where thicker ductile films can withstand higher

11

strains before the normalized resistance deviates from the theory [39]. The films would thus be expected to follow close to the theory line due to the thickness.
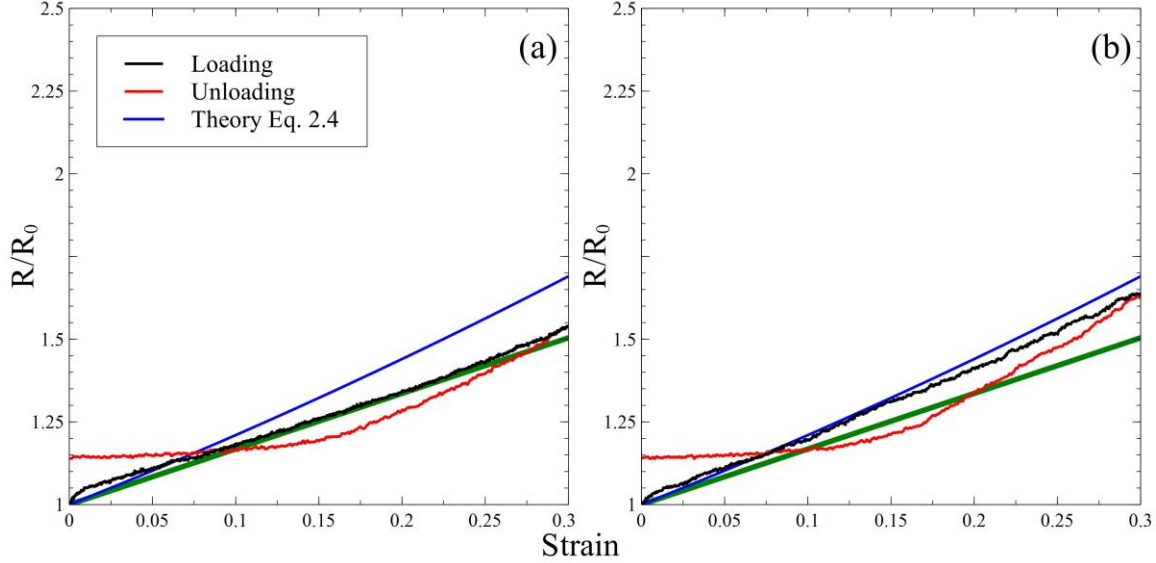
Fig. 2.2: The characterization of the change in normalized resistance during applied tensile load (black line) and unloading (red line) is compared with the theoretical model (blue line). In particular, the influence of interlayers on the Ag film normalized resistance-strain is demonstrated within graphs (a) and (b). The system structures for the respective graphs were: (a) 900 nm Ag/Kapton, (b) 900 nm Ag/ 45 nm Ti/ Kapton. The graphs show the increase in normalized resistance upon loading of the samples and the decrease to a magnitude above the initial upon unloading.

While the decrease in normalized resistance is expected upon unloading, the tendency of the curves to drop below the theory line is difficult to explain as this behavior could be due to vacancy removal or grain growth. Both of these possibilities are difficult to provide evidence for, as they would require complicated in-situ experiments, such as neutron scattering or EBSD. After unloading, the magnitude of the normalized resistance would be expected to drop further until the viscoelastic recovery of the polymer substrate is complete [47].

When loading remains very close to the theory line, it should not be assumed that no deformation occurs. Other in-situ studies (SEM, AFM, CLSM) have shown that ductile films do plastically deform under tensile strain at low strains, but the electrical response is not influenced. Such a study has been shown by *Berger et al.* [46] for 200 nm thick Cu films strained with in-situ AFM imaging. Therefore, one should not say that the films can withstand 30% strain without deformation. This is the reason for further study into the methods of measuring electro-mechanical properties of ductile films.

Looking at the inclusion of a Ti interlayer, the films on the Kapton substrate do not appear to have been affected much with regards to the normalized resistance curve. Although (b) has a slightly higher normalized resistance at 30% strain, both curves decrease to R/R_0 values of approximately 1.15. Others have found that adhesion interlayers are actually detrimental to the electro-mechanical behavior [43]. Similar behavior is not observed here most likely due to the film thickness of the Ag layer. The interlayer affects ductile films 200 nm and less, here they are 900 nm. However, the SEM images do show different cracking behaviors (Fig. 2.3).

Localized deformation and cracking in the strained films can be seen in Fig. 2.3. The SEM images demonstrate that, even though the normalized resistance plots do not deviate from the theory line given by Eq. 2.4, there is plastic deformation and cracking occur in the films. Films with an interlayer exhibited more cracking across the films suggesting that the interlayer may reduce the electro-mechanical properties. In films with and without an interlayer cracking was observed, and in both film systems the cracking was not observed to be constant across the films. The observation coupled with the

13

normalized resistance plots may suggest that the critical point has not been reached for these film systems where cracking of the film is significant enough to influence the normalized resistance across the films.
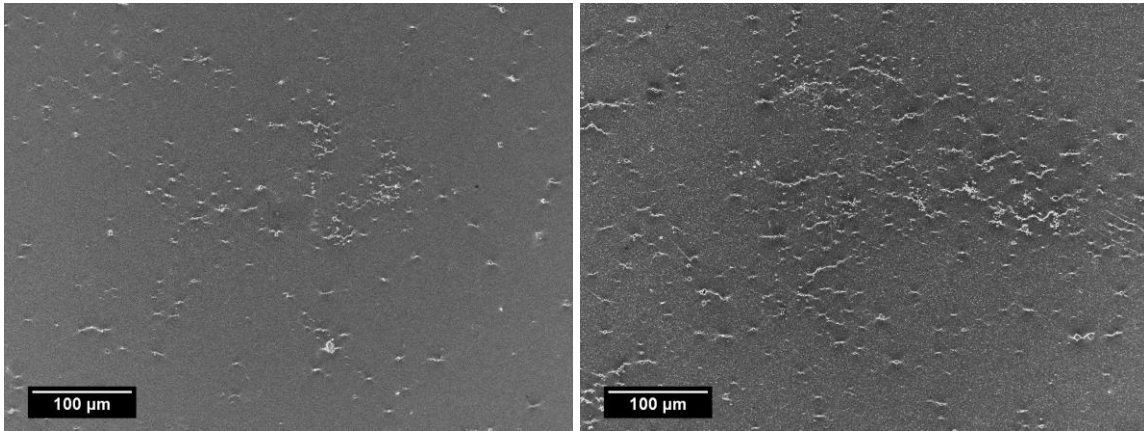
Fig. 2.3: SEM micrographs of Ag/Kapton (Left) and Ag/Ti/Kapton (Right) that have subjected to monotonic tensile straining up to 30%. For both images the tensile straining direction is in the vertical direction. Both samples exhibited cracking in the films that appear to be localized in areas of defects in the films, however the film with the Ti interlayer has a larger density of cracks.

The cracking seen in Fig. 2.3 was also observed to occur generally in areas of surface defects, such as scratches and hillocks, in the film leading to small localized areas of cracks across the sample with large areas of the film devoid of cracks. These surface defects likely aided the initiation or propagation of the small cracks observed in these samples. Despite these defects being present in the films, neither film system was observed to have widespread cracking throughout the film.

2.3.2. Ag/PEN Films

The normalized resistance-strain curves for 900 nm Ag films on PEN is shown in Fig. 2.4. The loading and unloading curves for films with and without a Ti interlayer

were compared to the theory line given by Eq. 2.4. Both film systems exhibited the expected behavior of normalized resistance increasing upon loading and decreasing to a value above the initial upon unloading. However, the normalized resistance curves deviated from the theory line at 12.5% and 5% strain for the Ag/PEN and Ag/Ti/PEN films, respectively. The deviation from the theory could indicate that the films had reached a critical crack density at which point factors other than strain of the film become more influential. In order to determine the contributing factors to this deviation, a more specific study with multiple in-situ methods would be required. The deviation strains, in this case, most likely correspond to a large enough through thickness crack density to cause a change in the electrical behavior and should not be considered a "fracture strain." But, clearly the Ti interlayer does improve the deviation strain.

The unloading behavior of the film without an interlayer was similar to other tests with the unloading curve dropping below the loading curve before plateauing. However, the unloading curve of the film with an interlayer followed the loading before beginning to plateau at approximately 20% strain. This could be due to cracks in the film being unable to bridge and the decrease being caused by the decrease in gauge length and/or microstructural changes in the film. A large difference between the R/R_0 values for the film systems was observed. The Ag/PEN film and Ag/Ti/PEN film had final R/R_0 values of approximately 1.36 and 1.71, respectively. The difference could indicate that there are fewer through thickness cracks or less re-bridging of cracks.
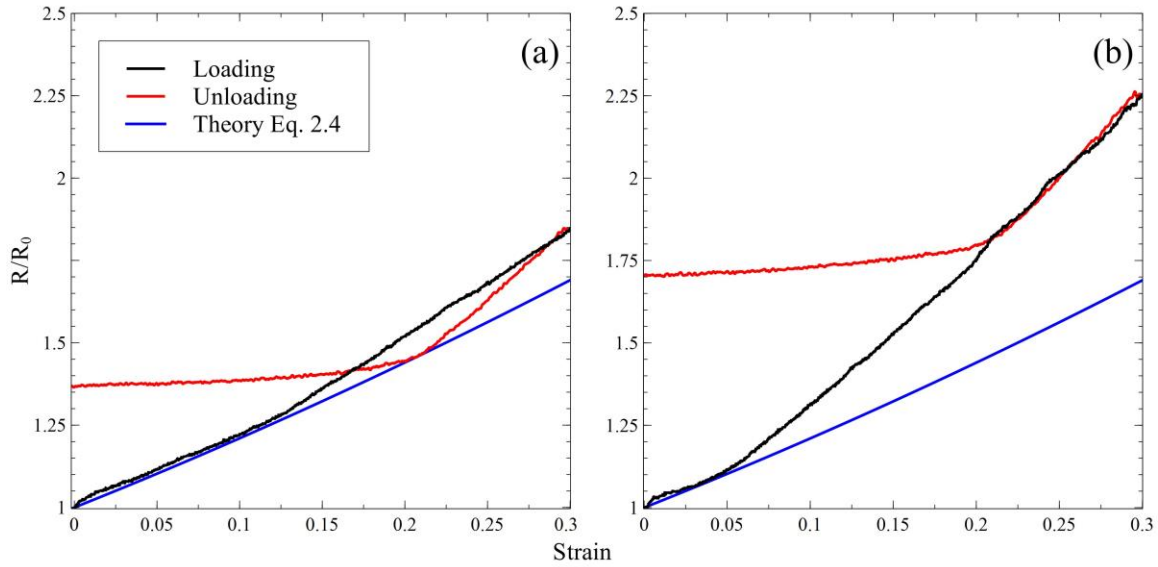
Fig. 2.4: The change in normalized resistance during monotonic tensile straining is compared to the theory line given by Eq. 2.4 is shown. In particular, the influence of a Ti interlayer is shown for the film systems of: (a) 900 nm Ag/PEN and (b) 900 nm Ag/ 45 nm Ti/PEN. Both film systems show an increase in normalized resistance upon loading and a decrease upon unloading to a magnitude above the initial value. Additionally, both curves exhibit a distinct deviation from the theory line at strains of approximately 12.5% and 5% for (a) and (b) respectively.

The cracking behaviors of Ag/PEN systems with and without an interlayer are shown in Fig. 2.5. Cracking was observed in films with and without an interlayer, but in films with an interlayer, there were many cracks that were accompanied by buckles. The buckles were induced during the unloading and form because the film goes into compression. In addition to buckles, the Ag/Ti/PEN samples exhibited more cracks than the samples without an interlayer. These observations add to the suggestion that thin interlayers that are typically deposited to aid in adhesion of the primary film to the substrate can be detrimental to the electro-mechanical performance of the films, and in this case, also do not improve the adhesion.
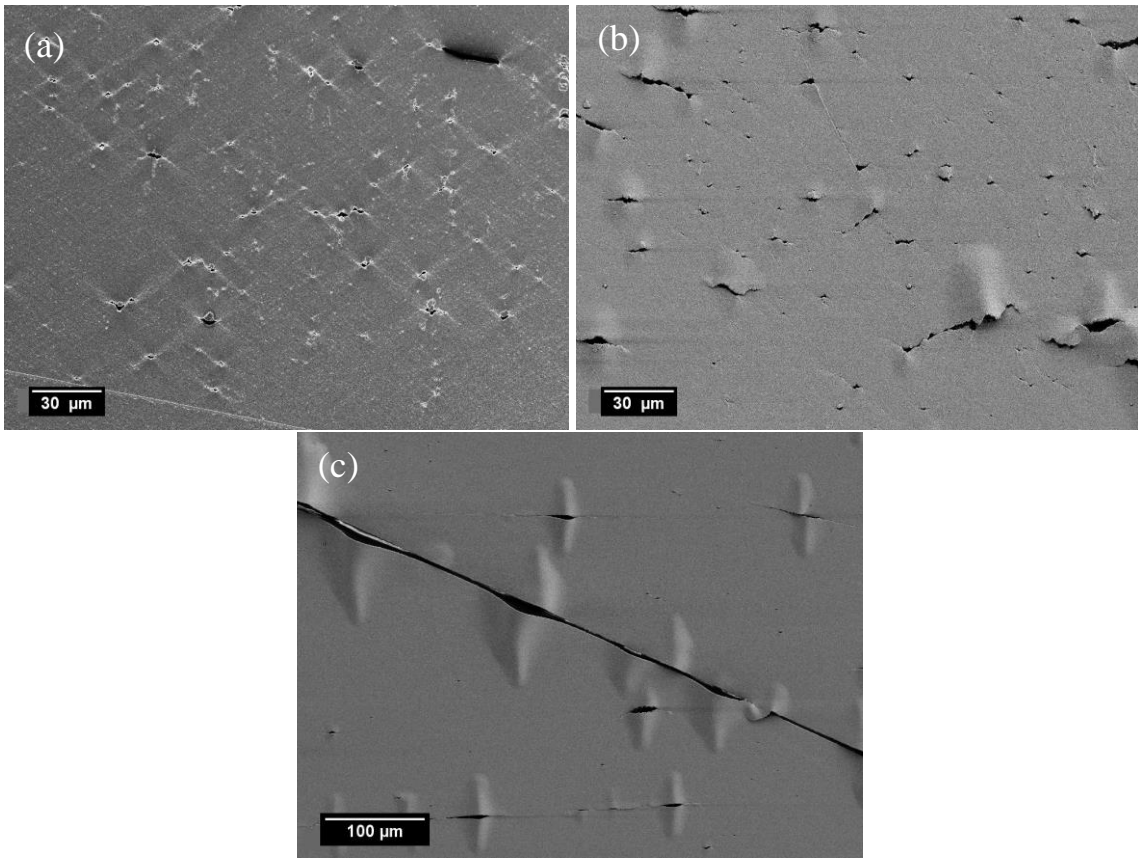
Fig. 2.5: SEM micrographs for Ag/PEN (a) and Ag/Ti/PEN (b-c) that have subjected to monotonic tensile straining. For both images the tensile straining direction is in the vertical direction. Cracking was observed in both film systems, but in the films with an interlayer, a significant amount of delamination accompanied an increased amount of cracks compared to the films without an interlayer.

When examining the cracking in some of the samples, there were cracks that appeared to be caused by scratches in the substrate. These cracks were distinct, straight lines that appeared to open along specific paths. The cracks may have also had an effect on the electrical behavior of the films during straining as many of the cracks were long, and some of the cracks were observed to span more than 1 mm across the length.

17

2.3.3. Ag/PET Films

The electrical behavior of Ag/PET films is shown in Fig. 2.6. The films with and without an interlayer demonstrated nearly identical behavior that closely followed the theory line given by Eq. 2.3 with the Poisson's ratio assumed to be $\nu = 0.37$ for PET. It is not yet fully understood why these film systems tend to follow this version of the theory, but this may be due to assumptions made in Eq. 2.4 being incorrect for these film systems. During the initial loading of the samples, a fast growth of R/R_0 was observed for the first 1-2% strain before the magnitude would return to the theory line at approximately 4% and 6% for the Ag/PET and Ag/Ti/PET systems, respectively. The observed behavior was also exhibited by samples on different substrates, so this behavior may be characteristic of the Ag films but needs to be investigated further to understand the causes.
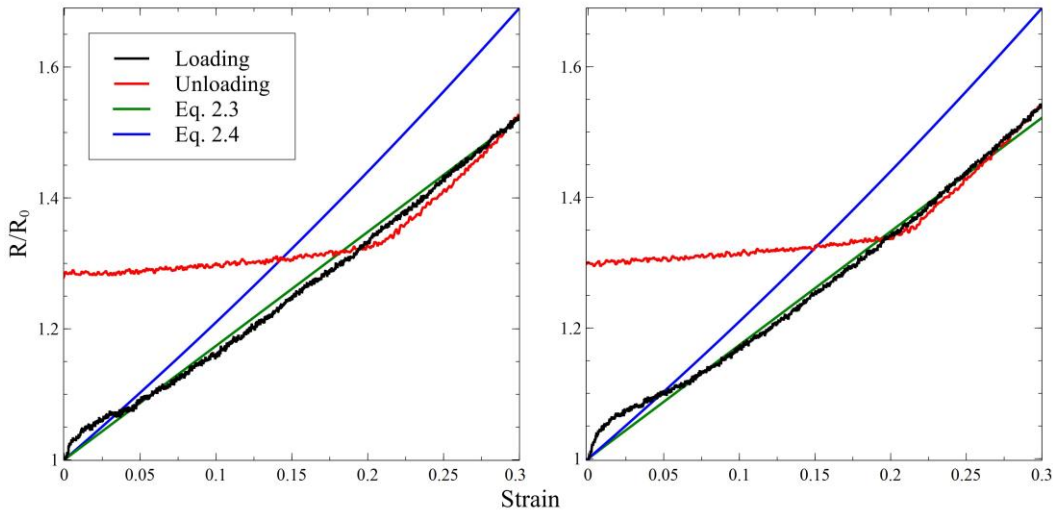
Fig. 2.6: The change in normalized resistance during monotonic straining of Ag/PET (Left) and Ag/Ti/PET (right). The loading (black) and unloading (red) curves are compared to the theory lines given by Eq. 3 (green) and Eq. 4 (blue). For Eq. 3, Poisson's ratio is assumed to be $\nu = 0.37$. Both films appear to follow the theory line given by Eq. 3.

During unloading, R/R_0 nearly follows the loading line unlike other substrates, which generally saw a drop in resistance below the loading curve or theory. For the films with and without an interlayer, the plateau of normalized resistance while unloading began at approximately 20% and the magnitude of R/R_0 after unloading was approximately 1.3.
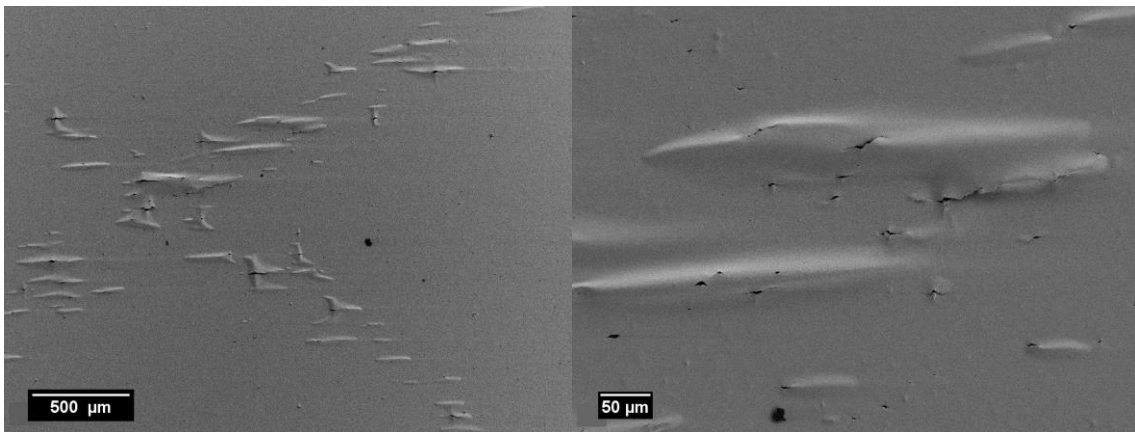
Fig. 2.7: SEM micrographs of compression buckling in Ag/Ti/PET films upon unloading in monotonic tensile straining. The straining direction is in the vertical direction of the micrographs.

After unloading, the Ag film with the Ti interlayer delaminated from the PET substrate as shown in Fig. 2.7. The buckles formed perpendicular to the straining direction because a compressive stress forms in the film as the load in removed and the substrate shortens. Because the buckle form spontaneously, they can be used to measure the adhesion energy of the failing interface. The buckle dimensions directly relate to the critical buckling stress and the delamination driving, or residual, stress of the film at the interface. The stresses and the interfacial fracture energies can be calculated using the well-known Hutchinson and Suo model [48]. The method is based on the Euler beam

theory. The required inputs are the buckle height, δ, and the half buckle width, b, the film thickness, h, as well as the elastic properties of the film (elastic modulus, E, and Poisson's ratio, v) (Fig. 2.8). With these values the critical buckling stress, σ_b, and the driving stress, σ_d, can be calculated by using [48].

$$\sigma_b = \frac{\pi^2 E}{12(1-v^2)} \left(\frac{h}{b}\right)^2 \tag{2.5}$$

$$\sigma_d = \sigma_b \left[\frac{3}{4}\left(\frac{\delta}{h}\right)^2 + 1\right]. \tag{2.6}$$

The critical buckling stress is the stress necessary to cause film delamination and the driving stress propagates the buckles. The interfacial fracture energy, $\Gamma(\Psi)$, for spontaneous buckles is given as

$$\Gamma(\Psi) = \left[\frac{(1-v^2)h}{2E}\right] (\sigma_d - \sigma_b)(\sigma_d + 3\sigma_b) \tag{2.7}$$

and is used to calculate the adhesion energy of the interfaces.
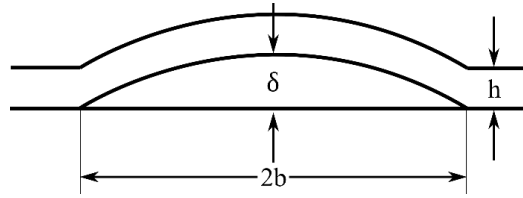
Fig. 2.8: Schematic diagram of a buckle cross-section showing the measurements of buckle height, δ, buckle width, $2b$, and film thickness, h.

Buckle dimensions can be measured using atomic force microscopy (AFM) or confocal laser scanning microscopy (CLSM). AFM is limited to buckle heights of approximately 2 μm and scan sizes of about 80 μm, while CLSM can be used to measure much larger areas (cm^2) and displacements (up to 1-2 mm). Smaller buckles were imaged using the

available AFM (Figure C). Only small buckles were measured because the majority of the buckles were too large for the AFM, thus requiring CLSM. From the AFM height images, the buckle dimensions were measured and used in Equations (2.5-2.7) to calculate the mixed mode adhesion energy. For the Ag/Ti/PET system, a $\Gamma(\Psi) = 60$ Jm^{-2}. The value is high compared to metal-ceramic interfaces, but in the right range for ductile metal-polymer systems [45, 49, 50]. Cross-sectioning of the buckles was performed with FIB to determine the failing interface. Figure 2.9 illustrates that the Ti-PET interface failed.
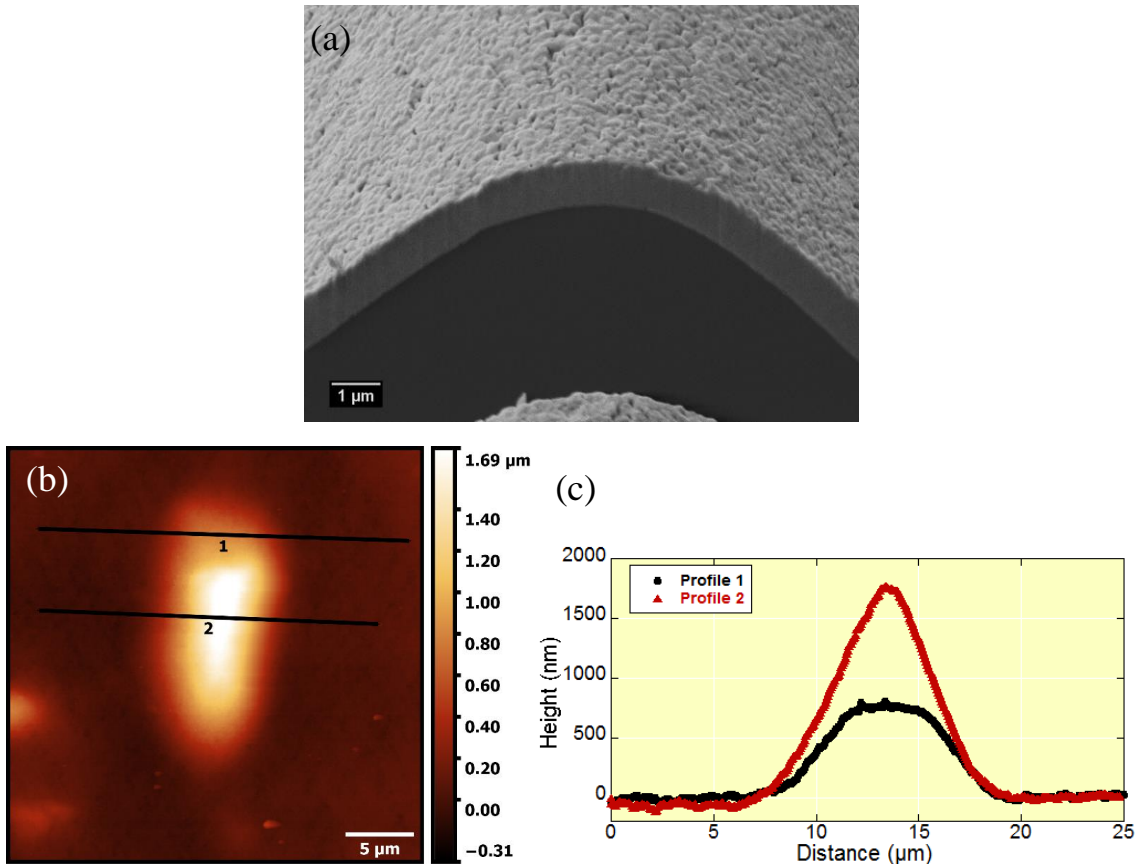
Fig. 2.9: Buckling in Ag/Ti/PET analysis was performed using FIB and AFM. (a) FIB cross-section of a Ag/Ti/PET buckle illustrating that the Ti-PET interface failed. (b) AFM height image of a small buckle that formed in the Ag/Ti/PET film. Two profiles are marked and shown in (c).

21

2.3.4. Printed Ag Films

In Fig. 2.10, the relationship between normalized resistance and engineering strain is shown for printed Ag lines subjected to uniaxial tensile load. The loading and unloading curves are compared to the theory line given by Eq. 2.4, which was derived in Section 2.1. Upon loading of the film, the normalized resistance follows the theory line before deviating at approximately 3% strain. This deviation is typically due to the initiation and propagation of cracks in the film since printed Ag films are brittle. The normalized resistance continues to increase during loading, and upon unloading, the normalized resistance begins to recover due to elastic recovery and crack re-bridging.
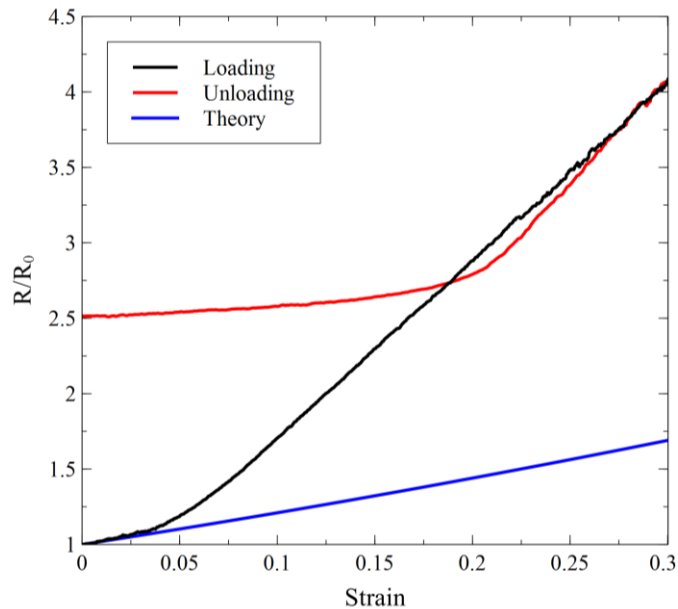
Fig. 2.10: Characterization of the printed Ag lines change in normalized resistance during applied tensile load (black line) and unloading (red line) is compared with the theoretical model (blue line). At small tensile strains during loading, the system performed close to the predictive model. The relative resistance deviated at 3% strain due to the initiation and propagation of cracks within the film. Upon unloading, the normalized resistance initially decreased rapidly until approx. 17.5% strain when the normalized resistance began to plateau.

The normalized resistance decreases as the gauge length decreases and cracks begin to close, but at approximately 17.5% unloading strain the curve begins to plateau indicating that plastic deformation had occurred in the substrate. As unloading continues, some cracks close or create bridges across the cracks further decreasing the resistance. After unloading, the normalized resistance would be expected to decrease further as the viscoelastic relaxation of the substrate would continue as explained in [47]. Despite this additional decrease, the normalized resistance would still be larger than the initial value due to cracks remaining open and the plastic deformation of the sample. The cracking behavior of the printed Ag lines can be seen in Fig. 2.11 (a) and (b). It can be seen many cracks formed during loading of the films and the propagation of the cracks appears to be assisted by the pores in the film.
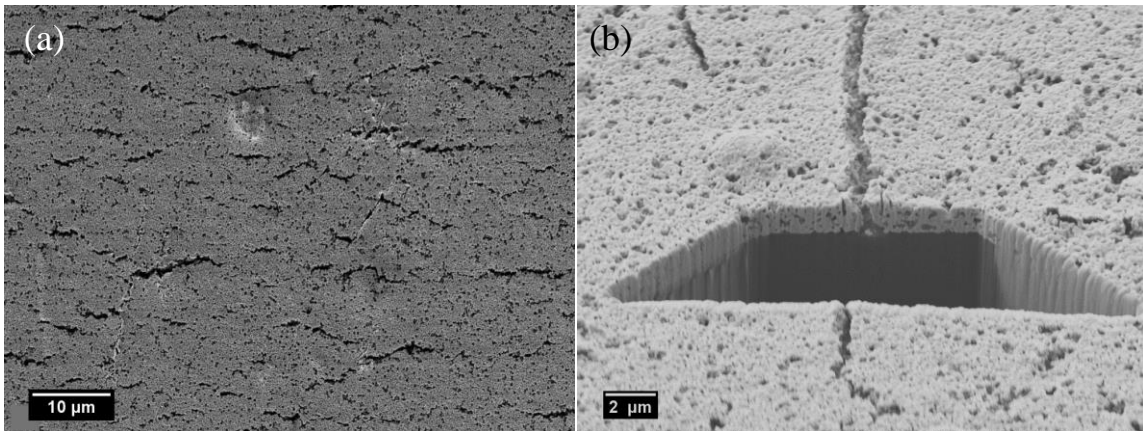
Fig. 2.11: The SEM images of the cracking behavior of printed Ag lines after monotonic tensile loading and unloading. The image on the left illustrates that many cracks in the film remain open after unloading leading to higher normalized resistance. The image on the right is a FIB cross-section of a through-thickness crack in a printed Ag line showing the brittle nature of the film. ((b) Image credit: Dr. A. Lassnig)

2.4 Summary of Monotonic Tensile Straining

Ag films sputter-deposited onto polymeric substrates with and without Ti adhesion layers along with printed Ag lines were subjected to monotonic tensile straining. In 900 nm Ag films, the addition of a Ti interlayer has been observed to be potentially detrimental to electro-mechanical behavior. In Ag/Kapton films, the inclusion of an interlayer was observed to cause more cracking and larger magnitudes of R/R_0 at maximum strain. Similarly, in Ag/PEN films, the inclusion of an interlayer caused more cracking, was observed to have higher values of R/R_0 at maximum strain and after unloading, and lower deviation strains. Additionally, buckling was observed in the Ag/Ti/PEN films suggesting that the interlayer may not be beneficial to the adhesion of the primary Ag film to the polymer substrate. This poor adhesion was also apparent in Ag/PET systems in which the films with an interlayer exhibited compression buckling upon unloading. In Ag/PET systems, the electrical behavior was not shown to be noticeably affected by the inclusion of an interlayer, but the buckling behavior could prove detrimental if it is also observed in other testing.

Printed Ag lines that were subjected to monotonic tensile testing exhibited contrasting electro-mechanical behavior to the PVD films. The printed Ag lines had an observed deviation strain at 3% strain and R/R_0 values at maximum strain and after unloading of 4.1 and 2.5, respectively. The deviation strain was lower than any of the PVD films and the values for R/R_0 were much higher. This contrast is due to the method of deposition and structure of the film that results in a brittle film that forms through

thickness cracks at low strains. The behavior aligns with previous work that has also shown that printed Ag films fail electrically at low strains due to the brittle nature [51]

Further experiments are necessary to complement the in-situ four-point-probe experiments that have been conducted and to better understand the behavior of the films. Additional experiments that are planned for the future include in-situ XRD, in-situ SEM, in-situ AFM, and in-situ CLSM. The XRD and CLSM experiments will be conducted with four-point-probe, and the AFM and SEM experiments will be used to correlate to existing data. These experiments could not be run during the stay due to time constraints, instrument availability, or lack of access to instrumentation (for examples XRD at a synchrotron source in Berlin, BESSY II). The experiments will serve to help determine the effectiveness of in-situ four-point-probe experiments for ductile films.

CHAPTER THREE

Electromechanical Response to Cyclic Tensile Testing

3.1. Introduction to Uniaxial Cyclic Fatigue of Metallic Films on Polymeric Substrates

Flexible electronics are designed to withstand stretching and bending strains that may be part of the lifetime of a device. The expected strains in a device can vary based on the application of the device, but the device must still maintain a certain level of performance during and after straining. In testing of thin films on polymers, traditional strain to fracture tensile testing is not always reliable as the polymer substrates prevent the localization of strain in the film making the failure mechanisms more complicated [36]. In order to test the reliability and lifetime of the thin films on polymer substrates for flexible electronics, cyclic fatigue experiments can be used with low strains of 1-2% that can mimic some expected strains in applications. Often fatigue experiments are performed using bending mode fatigue, but with the development and interest in more stretchable electronics uniaxial cyclic fatigue tests have been used as well [36, 41]. In these experiments, electrical measurements are made in-situ not only to observe the evolution of the resistance but to help determine when failure may be determined to occur.

3.2. Experimental Methods

3.2.1. Cyclic Tensile Testing

Cyclic tensile fatigue testing was performed using a MTS Tytron 250 with a four-point probe set-up incorporated into the sample grips to measure changes in resistance

across the film in-situ with a Keithley 2000 multimeter at the Erich Schmid Institute of Materials Science in Leoben, Austria. More information on the set up can be found in [36]. Samples for testing were sectioned to dimensions 5 mm by 35 mm with a gage length of 15 mm. Tests were performed with a frequency of 0.1 Hz and a maximum strain of 2% for cycles of 5,000 and 10,000 cycles. The dimensions and loading parameters for this testing were chosen to be similar to [36]. Sample system and number of cycles used in cyclic tensile testing are indicated in Table 3.1. With these film-substrate systems the role of substrate, deposition methods and adhesion interlayers were studied.

Table 3.1: The cyclic testing was performed on Ag films deposited with and without Ti interlayers on a range of substrates.

Film	900 nm Ag		900 nm Ag/ Ti		1.8 μm Ag	
Cycles	5,000	10,000	5,000	10,000	5,000	10,000
Substrate						
PI Sheet	x	x	x	x	x	x
PEN	x	x	x			
PTFE	x					
	1.25 μm Printed Ag					
PET		x				

3.3. Results and Discussion

    3.3.1. Ag/Kapton Films

Cyclic tensile fatigue tests were performed on several film systems and the typical profile of the normalized resistance vs. cycles curves for film systems on Kapton are shown in Fig. 3.1. Fig. 3.1 (a) shows the cyclic normalized resistance curve for 900 nm Ag/Kapton over 10,000 cycles and (b) shows the individual cyclic profile for the system. As the samples are loaded, the stretching of the film causes an increase in normalized

resistance, but the formation and propagation of cracks also contributes to this increase. When the samples are unloaded, the normalized resistance decreases due to the decrease in gage length and cracks closing. However, the unloaded normalized resistance also continues to increase after cracks have formed since the through thickness cracks cannot fully close or increase in length.

Compared to the film with a Ti interlayer (c) and the thicker film (d), the Ag/Kapton film exhibits a smaller amplitude. This smaller amplitude may suggest that the average crack length and density in the 900 nm Ag/Kapton is smaller than Ag/Ti/Kapton and 1.8 μm Ag/Kapton samples. At 10,000 cycles, the amplitude for the Ag/Kapton sample in Fig. 3.1(a) is approximately 0.4, whereas the amplitudes for the curves in (c) and (d) are approximately 1.8 and 2.3, respectively.
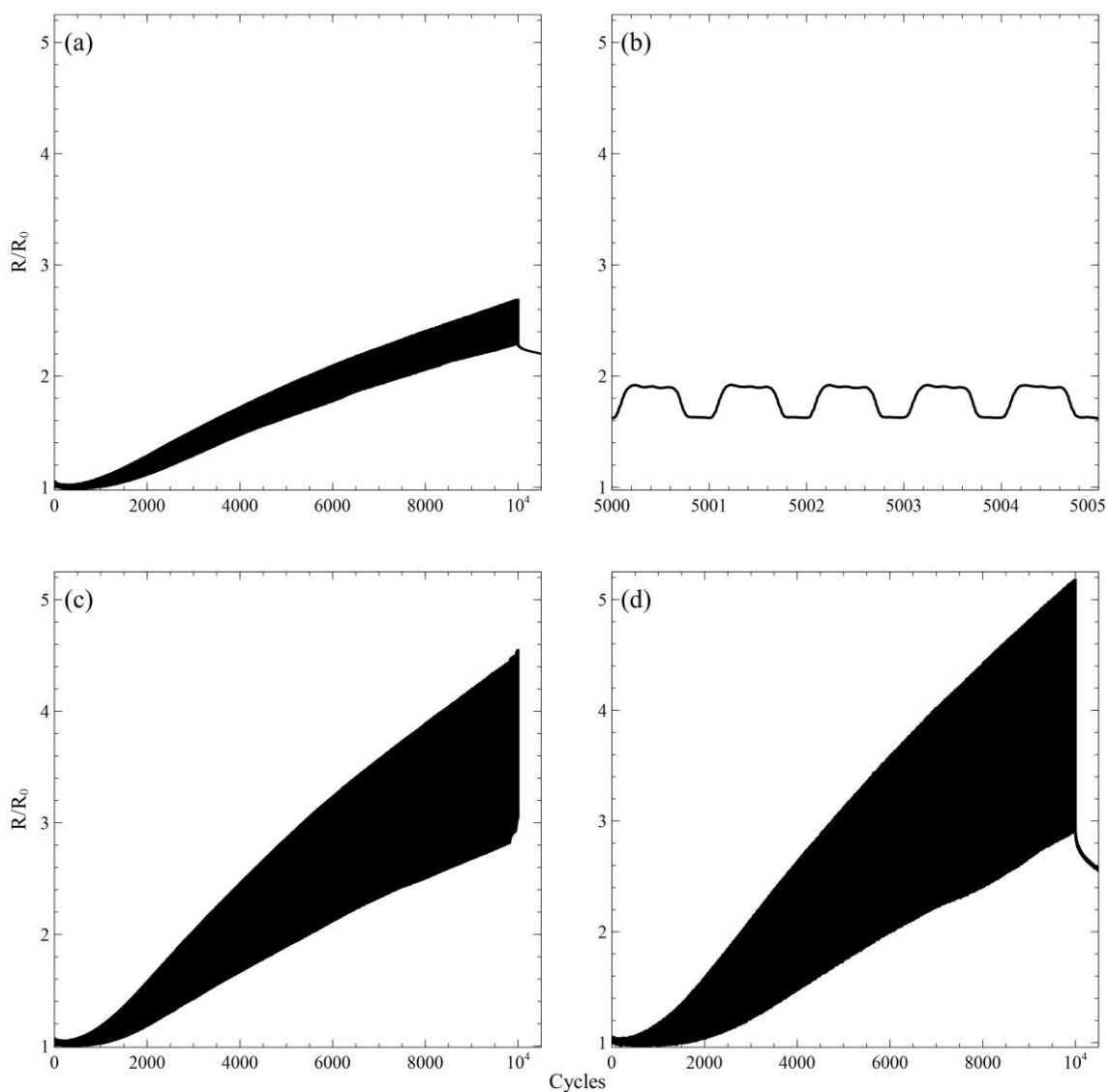
Fig. 3.1: The impact on the normalized resistance of Ag films during cycling was monitored for systems with and without interlayers and two. These graphs (a-d) reflect the performance of systems with Kapton substrates during 10,000 cycles. The normalized resistance spread for each cycle reflects the fluctuation between loading and unloading in tension. The system compositions for the graphs were: (a-b) 900 nm Ag on Kapton where (b) is a zoomed in profile at 5,000 cycles, (c) 900 nm Ag on Kapton with Ti interlayer, (d) 1.8 μm Ag on Kapton. The graphs indicate that systems with thicker films (1.8 μm relative to 900 nm) and those with an interlayer exhibit a larger amplitude for normalized resistance and a larger increase in unloaded normalized resistance than the 900 nm Ag film (a). The data points beyond 10,000 cycles show the relaxation of the film following unloading.

29

In Fig. 3.2, a comparison of the individual cycle profiles for the three previously shown film systems (900 nm Ag/Kapton, Ag/Ti/Kapton, and 1.8 μm Ag/Kapton) can be seen. The profiles seen in 3.2(a) show that the normalized resistance curves for all of the film systems are similar during the initial cycling. As cycles increase, the differences between the film systems begin to appear. Shown in ##(b), at 2,500 cycles the amplitudes between all three systems become easier to differentiate. At this point, cracking of the films has begun as the profiles exhibit a more pronounced pattern of increasing and decreasing normalized resistance upon loading and unloading, which hints at the opening and closing of cracks.

The effect of film thickness and interlayers on normalized resistance curves is apparent in Fig. 3.2(b) and (c) as the amplitudes of the normalized resistance for those systems increase over cycles. At higher cycles, the shape of the normalized resistance at the maximum strains was noticeably different. The nonlinear behavior at these strains is not fully understood, but this could be related to cracking events or deformation of the polymer substrate. The film thickness and interlayer also appear to have varied effects on the electrical behavior of the films. While both show an increase in amplitude, the shape at maximum strain for the thicker film is a more pronounced version of the thinner film without an interlayer, and the film with an interlayer appears to exhibit a completely different shape. This could be due to a difference in cracking behavior caused by the interlayer, and to understand this behavior further, more in-situ imaging experiments will be required, such as in-situ AFM or SEM.
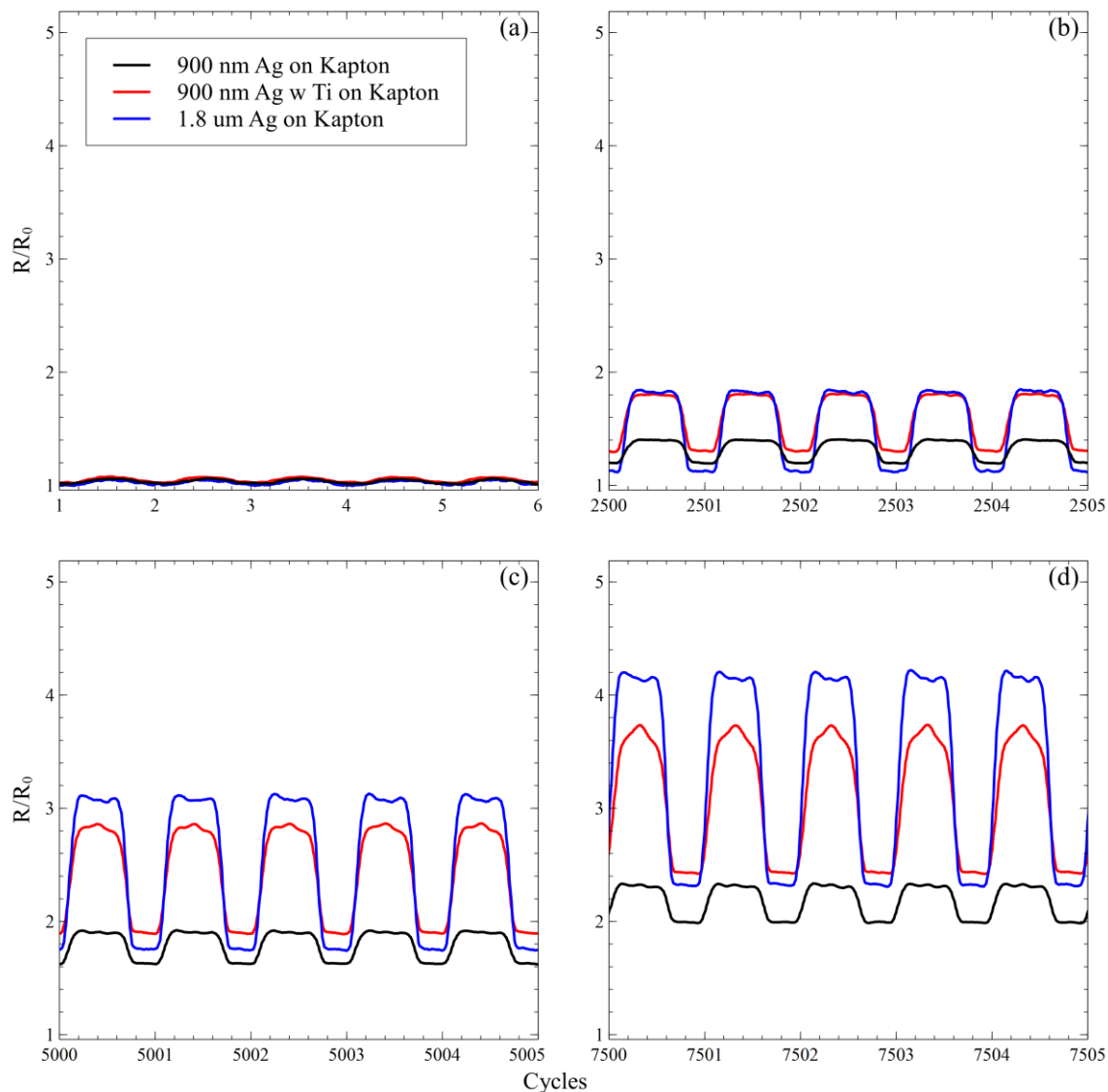
Fig. 3.2: The fluctuation of the normalized resistance at regions of the cyclic loading were examined as a function of film thickness and the inclusion of interlayers. The systems included are 900 nm Ag/Kapton (Black), 900 nm Ag/Ti/Kapton (Red), and 1.8 μm Ag/Kapton. (a) Shows that all film systems had similar normalized resistance with small normalized fluctuations. (b-c) show that the films with the interlayers and higher thicknesses have greater normalized resistance magnitude changes.

The cracking behavior of the 900 nm Ag/Kapton system is shown in Fig. 3.3. The film exhibited a large amount of jagged cracks that can be densely packed, but might not necessarily connect to make a network of cracks across the film. In addition, the 900 nm

31

Ag/Kapton was also observed to have formed extrusions that aid in the initiation and propagation of cracks across the film. While the film may appear to be heavily cracked, it must also be noted that many cracks in the film may not be through-thickness cracks, so upon loading the full width of the crack does not fully open leading to the smaller amplitude seen in the normalized resistance curves. The average linear crack density for the Ag/Kapton sample after 10,000 cycles was measured to be 3.75 x 10^{-2} cracks/μm.
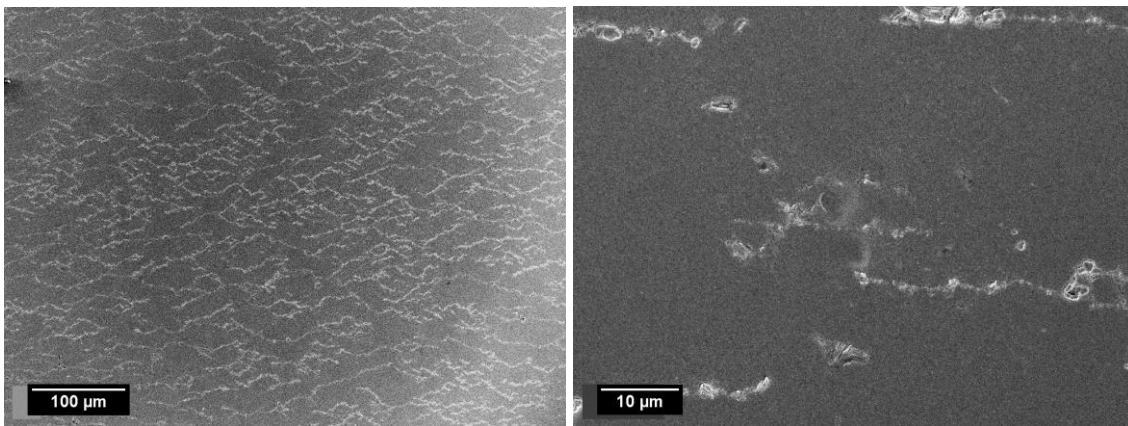
Fig. 3.3: SEM micrographs of 900 nm Ag/Kapton after cyclic tensile testing to 10,000 cycles. (Left) A micrograph demonstrating the general cracking behavior of short jagged cracks; (Right) A higher magnification micrograph that shows some extrusions between cracks and some as part of cracks.

For comparison, the cracking behavior of 900 nm Ag/Ti/Kapton and 1.8 µm Ag/Kapton films after 10,000 cycles of tensile straining can be seen in Fig. 3.4. In both films, long brittle cracks form, which can extend for hundreds of microns and no extrusions were observed to have formed. However, the film with the interlayer had a much higher average linear crack density of 4.81 x 10^{-2} cracks/μm compared to 2.78 x 10^{-2} cracks/μm in the 1.8 µm Ag/Kapton film. Larger crack spacing is apparent as well in the thicker film shown in Fig. 3.4. Pairing these observations with the electrical behavior measurements from these films it can be noticed that crack length must have a major role

in the electro-mechanical behavior. Although, a crack length or average crack length can be difficult to determine, especially with ductile films, because when imaging long cracks, getting a sufficient number into the images to have reliable data can be time-consuming and difficult. In ductile films, the problem lies with determining what cracks are through thickness cracks and what is the actual length of the cracks, since ductile films generally neck before failing. To have a reliable approximation for crack length, more in-situ imaging will be required.
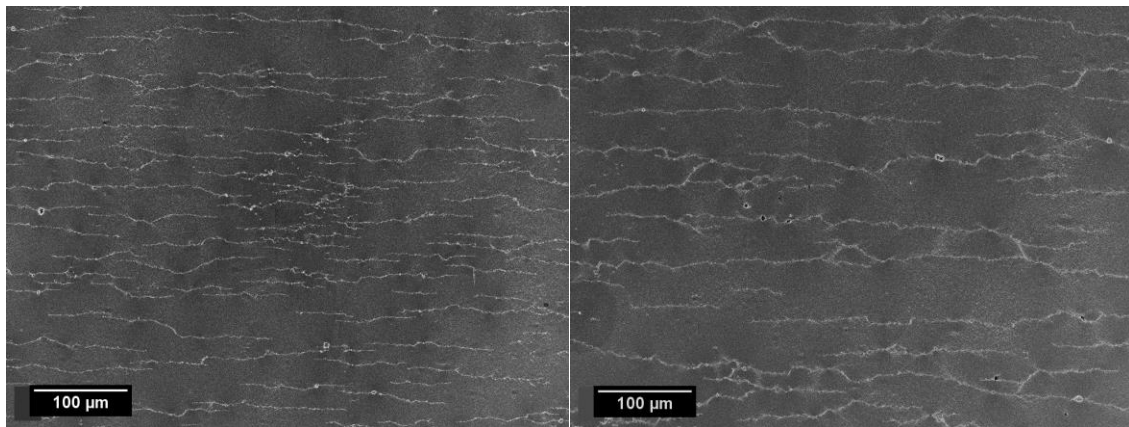
Fig. 3.4: SEM micrographs of 900 nm Ag/Ti/Kapton (left) 1.8 µm Ag/Kapton (right) after cyclic tensile testing to 10,000 cycles demonstrating the general cracking behavior of the films. Both films developed long cracks with some connecting.

The electrical behavior of the Ag/Kapton systems with and without an interlayer were compared by extracting the minima and maxima curves of the cyclic normalized resistance and is shown in Fig. 3.5. When compared this way, it can be seen that the minima of Ag/Ti/Kapton films do not vary much, but the maxima vary between the replicates. The minima of each of the replicates and the Ag/Kapton all share a similar profile, while the maxima curves all appear to have varying profiles. It is speculated that this could be due to differences in the opening of the cracks between the samples, but

different types of in-situ testing would be required to examine this possibility. These differences could also be related to differences in crack density and length, which could be brought on by differences in apparent defect densities between the samples.
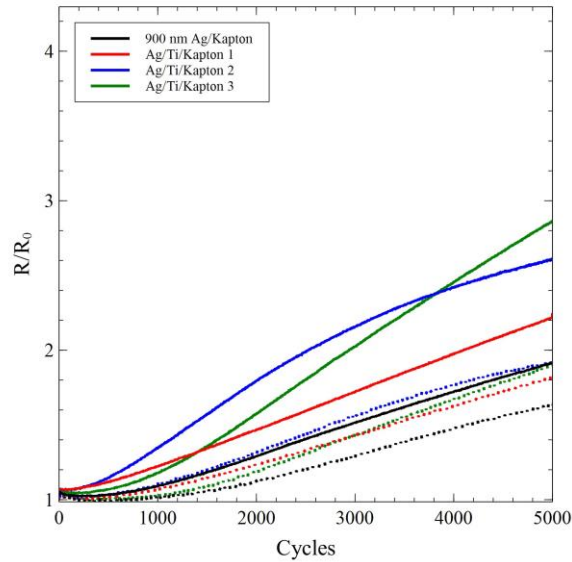
Fig. 3.5: Maxima and minima curves extracted from Ag/Kapton and Ag/Ti/Kapton cyclic tensile tests showed variation in normalized resistance as a function of cycles.

3.3.2. Ag/PEN Films

The change in electrical behavior during cyclic tensile testing for Ag/PEN films with and without an interlayer is shown in Fig. 3.6. It can be seen that both film systems take on similar profiles, but the film with an interlayer has a much higher amplitude at 5,000 cycles. The amplitude at 5,000 cycles of the Ag/PEN film is approximately 2.0 while the Ag/Ti/PEN film is approximately 4.5. This large difference could be due to a larger average crack density and crack length in the film with an interlayer. The minima of both systems appear to be similar suggesting that both films recover to around the

34

same point. Similar to the Ag/Kapton, the Ti layer appears to have more of an effect on the amplitude of the normalized resistance than the unloaded resistance.
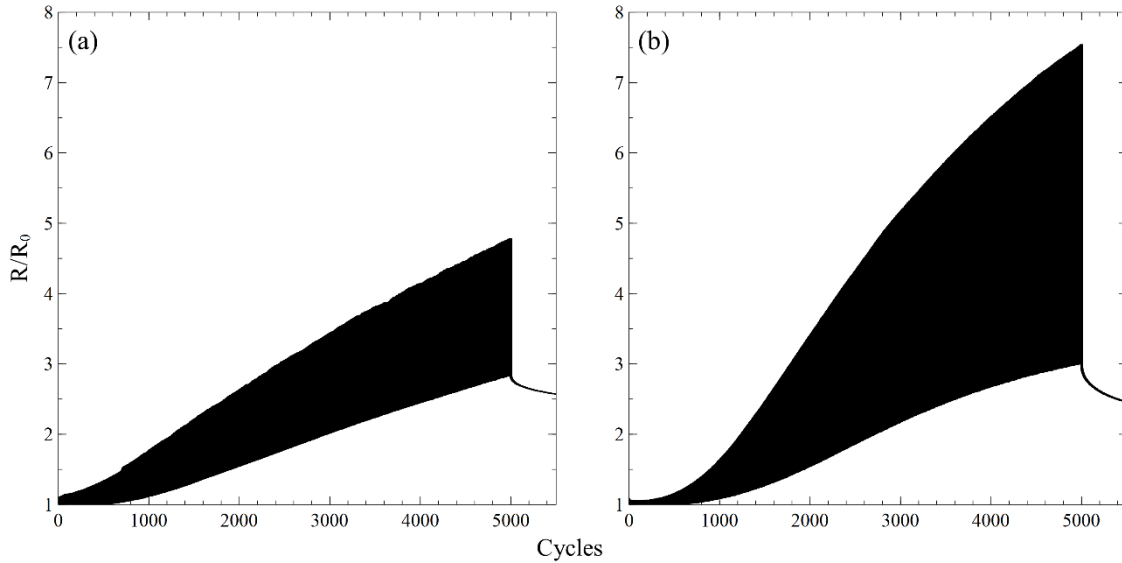
Fig 3.6: The influence of an interlayer on the normalized resistance during cyclic tensile tests up to 10,000 cycles in the film system on PEN can be seen by comparing (a) and (b). The compositions for the graphs are: (a) 900 nm Ag and (b) 900 nm Ag with Ti interlayer. The comparison between (a) and (b) suggests that the addition of an interlayer caused an increase in the amplitude of the normalized resistance. The minima of the normalized resistance do not appear to have been affected.

The cracking of these films after cyclic tensile straining is shown in Fig. ##. The Ag/PEN sample exhibited a mixture of long straight cracks and short jagged cracks with extrusions. The surface appeared to be dominated by the regions of short cracks and extrusions, but it is uncertain as to why there are two clear types of regions that have different cracking, but this may be tied to the properties or quality of the substrate. Extrusions can be seen primarily in areas of the shorter cracks on the Ag/PEN film. In contrast, the Ag/Ti/PEN sample exhibited very few areas of short cracks and extrusions and was primarily covered by long brittle cracks that were expected to be seen due to the

inclusion of the Ti interlayer. The areas that appear to be extrusions in the Ag/Ti/PEN film may also just be areas of surface defects and would require SEM to determine the nature of these areas. It is still interesting that films with and without an interlayer may exhibit the same types of cracking as the Ag/Ti/Kapton films did not exhibit any extrusions, and, in general, films with a brittle interlayer would only be expected to form cracks and not extrusions. Though, a tendency primarily to form brittle cracks could still explain the large differences in the amplitudes observed in the normalized resistance plots.
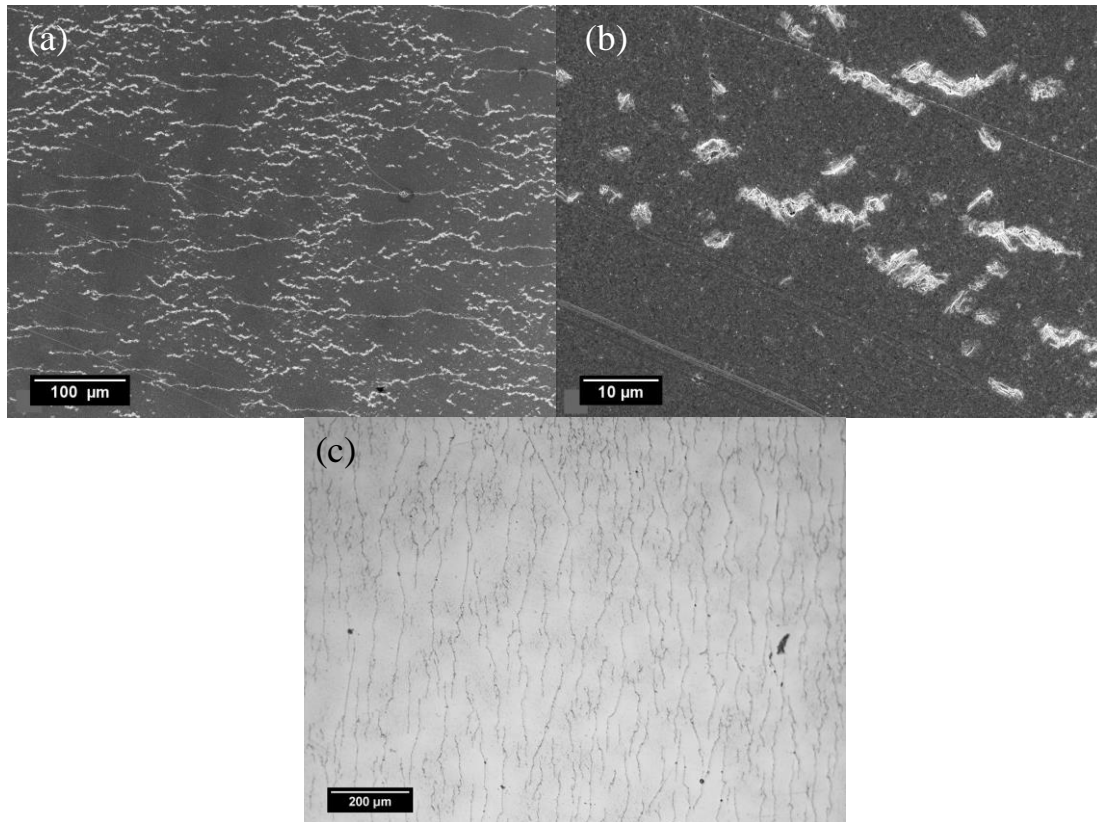
Fig. 3.7: (a-b) SEM micrographs of Ag/PEN after cyclic tensile testing to 5,000 cycles. The image on the left is an overview of the general cracking behavior, and the image on the right shows some of the extrusions seen throughout the sample surface. The straining direction is in the vertical. (c) An optical micrograph of the cracking in Ag/Ti/PEN after

36

5,000 cycles. The straining direction is in the horizontal. The surface shows primarily long brittle cracks with few extrusions.

The curves of the maxima and minima of the cyclic normalized resistance for Ag/PEN film systems were extracted for comparison and shown in Fig. 3.8. For the tested samples shown, the minima appear to be unaffected by the inclusion of a Ti interlayer. As seen previously, the maxima of the Ag/Ti/PEN film are much larger than those of the films without the interlayer, but what is interesting is seeing the changes and differences between the film systems before 1,500 cycles. The Ag/PEN films exhibited higher normalized resistance and amplitudes, while the Ag/Ti/PEN appeared to slightly decrease in normalized resistance in the first 400 cycles before increasing and becoming larger than the Ag/PEN tests after about 1,000-1,400 cycles.
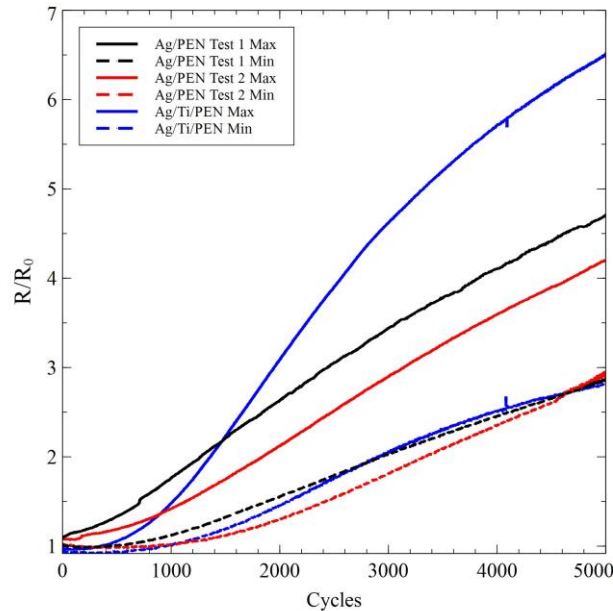
Fig. 3.8: The maxima and minima curves of extracted from the cyclic normalized resistance plots of Ag/PEN and Ag/Ti/PEN film tests. The solid lines represent the

37

maxima and the dashed lines represent the minima extracted from the cyclic resistance plots.

3.3.3. Printed Ag Films

The normalized resistance curve and individual cycle profiles of printed Ag lines subjected to cyclic tensile testing is shown in Fig. 3.9 (a) and (b) respectively. The behavior of the films was very different in overall shape and individual profiles than the previously examined sputtered films. The overall curve shows a dramatic increase in normalized resistance from the start and appears to begin to level off after 2,000 cycles suggesting that the resistance may reach a saturation point. The individual profiles of the cycles had a rounded shape at the peak loads and the amplitude of the cycles never appear to increase beyond approximately 1.0.
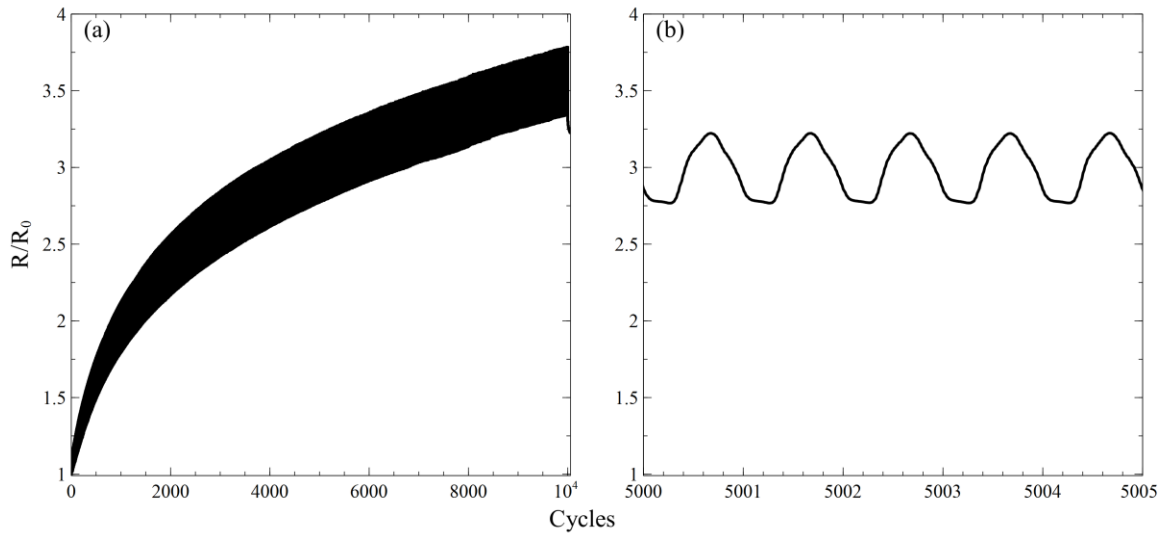
Fig. 3.9: The normalized resistance for printed Ag films was monitored for 10,000 cycles and shown in (a). The profile of individual cycles after 5,000 cycles can be seen in (b).

While different, the electrical behavior of the films is not surprising considering the method of deposition. Differences between PVD films and printed films have been shown in many studies [36, 29, 52]. The films tend to have a different microstructure than PVD films due to the deposition process. As seen in Section 2.3.4, the films are porous and also behave differently in the monotonic straining process. In the cyclic straining process, the strains are much smaller, so the types of cracking seen in those tests was not anticipated. The cracking behavior for the printed Ag films after cyclic tensile testing is shown in Fig. 3.10, and demonstrates another major difference between the printed and PVD films. Unlike in previous films, the cracks in the printed Ag are not oriented in any particular way with respect to the straining direction. Instead, the cracks appear to prefer propagating along pores in different directions. The way cracks initiate and propagate in the film are likely tied to the way the films were printed and more characterization and testing of these films will be needed.

Fig. 3.10: SEM micrograph of a printed Ag line after 10,000 cycles of tensile straining. Cracks are observed propagating in several directions and the direction of propagation appears to be independent of straining direction, which is in the vertical direction.

3.4. Summary of Cyclic Tensile Fatigue Testing

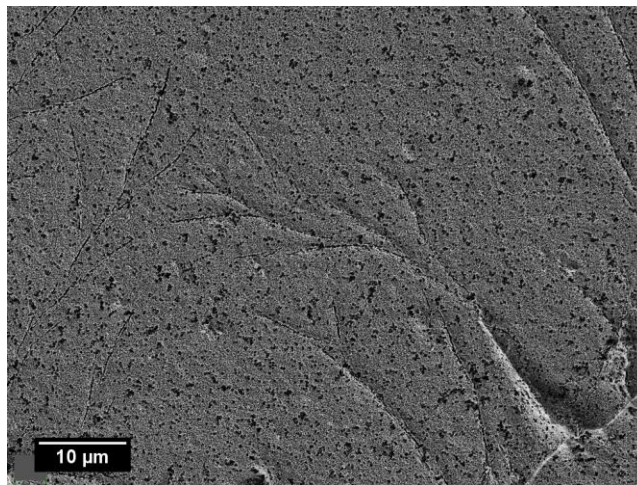Ag films sputter-deposited onto polymer substrates with and without Ti interlayers along with printed Ag samples were subjected to cyclic tensile testing for 5,000 to 10,000 cycles. In 900 nm sputtered films, the addition of a Ti layer was shown to be potentially detrimental due to large increases in normalized resistance when strained. In addition, an increase in film thickness to 1.8 µm also demonstrated large increases in normalized resistance upon straining. In films on Kapton, the amplitude of cyclic normalized resistance was approximately 0.4, 1.8, and 2.4 for 900 nm Ag/Kapton, Ag/Ti/Kapton, and 1.8 µm Ag/Kapton, respectively. These differences can be correlated to the cracking behavior in the films. The 900 nm Ag/Kapton film exhibited short jagged cracks with many extrusions that initiate cracks scattered throughout the film, whereas, the thicker film and Ag/Ti film exhibited long brittle cracks with no extrusions in the film. The linear crack densities measured for the samples were not consistent with what was anticipated. The densities were expected to increase with increasing resistance, but the film with the largest amplitude, 1.8 µm Ag/Kapton, was measured to have the lowest average linear crack density and the highest average linear crack density was the film with the interlayer. This observation shows that the length of the cracks likely has a large impact on the amplitude of the normalized resistance curves.

Similarly, Ag/Ti/PEN films were observed to have a much higher amplitude of the normalized resistance of 4.5 compared to 2.0 at 5,000 cycles for Ag/PEN, but the minimum value of resistance over 5,000 cycles remained similar for both film systems. The Ag/PEN film systems also demonstrated the expected cracking behavior to an extent,

but it was observed that the Ag/PEN film formed both short cracks from extrusions and long cracks that would be expected in samples with an interlayer. The trend of crack density was also odd, because despite the Ag/Ti/PEN exhibiting higher amplitude the average linear crack density of the Ag/Ti/PEN was lower than that of Ag/PEN after 5,000 cycles. This shows again the impact of the average crack length.

The printed Ag samples demonstrated the effects of deposition technique on the cyclic normalized resistance behavior. Printed Ag samples exhibited a different profile of the normalized resistance over 10,000 cycles than the PVD samples, which was not too surprising considering that the samples are printed. The unexpected part was that the cracking in the printed Ag propagated in several directions and seemed to be independent of the straining direction. This behavior is likely due to the printing process leaving pores and other defects that may be preferable for the cracks to propagate along. Further characterization of these printed films will be needed to fully understand the electro-mechanical behavior.

Further experimentation and analysis is needed to complement the work that has already been done with these samples. In-situ imaging (AFM, CLSM) with four-point-probe will be considered to view how cracks initiate and evolve during cycling, but these types of experiments are time-consuming. A limited amount of time or lack of access to the types of equipment required for these experiments made it difficult to consider during the contracted time period.

CHAPTER FOUR

Exploratory Experiments and Future Work

4.1. Exploratory Experiments

A number of exploratory experiments were run during time when equipment required for previous experiments was not accessible or as a proof-of-concept for future ideas. These experiments included bending fatigue tests, scratch tests, and a combination of scratch tests with bending and straining.

Flexible electronics are designed to withstand deformation and the most common form of expected deformation would be bending mode deformation. For this reason, cyclic bending fatigue is a well-studied topic, but the methods of bending vary between groups [34, 29, 27]. Methods in literature can use in-situ four-point-probe set-ups that allow for monitoring and evolution of the resistance as the sample is bent at certain bending radius, while others focus primarily on the cracking of the film. The bending experiments used the methods developed in [27] and a version of the methods described in [29]. The films explored for these tests were the Ag/Kapton and Ag/PEN systems with and without Ti interlayers and the printed Ag lines. For the films tested, the effects of the bending appeared minimal with the smallest bending radius available, and not much can be discerned. Although, the minimal effects may be due to the film thickness, so future experiments using these bending methods will center around thinner films. Thinner films will allow any potential effects of a brittle interlayer to be observed and may help highlight how printed Ag samples may be affected by bending fatigue.

Different methods of scratch testing were explored with Ag/PEN films to attempt to observe any effects scratching of the metal film may have on the electro-mechanical properties. Attempts were made using the FLEX-E TEST developed in [27] to scratch the metal films and determine if this affected the electrical behavior, but it was observed that the scratching alone did not have an effect. Further attempts combined scratching the surface in different orientations and subjecting the films to monotonic tensile straining or bending mode straining. The idea was to see if scratching the surface of the sample would affect the performance in these straining tests. Initial observations of this proof-of-concept method showed that in some orientations cracks preferentially form along scratches, but in some cases cracks may be prevented from propagating through the film by scratches. This was an interesting result that may be explored more in the future.

4.2. Future Work on Ag Films

The work performed as part of this program provided results that helped answer questions, but also raised many more. As mentioned in the previous chapters, numerous in-situ studies will be considered to further understand the electro-mechanical behavior of the films studied. In addition to uniaxial tensile straining tests, bending and scratch test combinations may also be explored further.

5. References

1. The Nielsen Company. "**The Total Audience Report Q4 2014**" (2015):

2. Future Market Insight. "**Consumer Electronics Market**" 44, no. 0 (2010): Available at http://search.ebscohost.com/login.aspx?direct=true&db=bth&AN=51790377&site=bsi-live

3. Shivakumar, S. J., Siegel, D. S., and National Research Council. "**The Flexible Electronics Opportunity**" (2014): National Academies Press.

4. Wong, W. S. and Salleo, A. "**Flexible Electronics: Materials and Applications**" (2009): doi:10.1007/978-0-387-74363-9Springer Science and Business Media

5. Harris, K. D., Elias, A. L., and Chung, H. J. "**Flexible Electronics under Strain: A Review of Mechanical Characterization and Durability Enhancement Strategies**" *Journal of Materials Science* 51, no. 6 (2016): 2771–2805. doi:10.1007/s10853-015-9643-3Springer US

6. Jain, K., Member, S., Klosner, M., and Zemel, M. "**Flexible Electronics and Displays : Lithography and Photoablation Processing Technologies for High-Throughput Production**" 93, no. 8 (2005):

7. Park, J., Kim, M., Lee, Y., Lee, H. S., and Ko, H. "**Fingertip Skin-Inspired Microstructured Ferroelectric Skins Discriminate Static/dynamic Pressure and Temperature Stimuli**" *Science Advances* 1, no. 9 (2015): e1500661–e1500661. doi:10.1126/sciadv.1500661, Available at http://advances.sciencemag.org/cgi/doi/10.1126/sciadv.1500661

8. Lee, J., Lim, Y., Park, C., Park, Y., Kim, C., and Hwang, Y. "**A-Si : H Thin-Film Transistor-Driven Flexible Color E-Paper Display on Flexible Substrates**" *Electron Device Letters* 31, no. 8 (2010): 833–835.

9. Kim, J., Hwang, J., Song, K., Kim, N., Shin, J. C., and Lee, J. "**Ultra-Thin Flexible GaAs Photovoltaics in Vertical Forms Printed on Metal Surfaces without Interlayer Adhesives**" *Applied Physics Letters* 108, no. 25 (2016): doi:http://dx.doi.org/10.1063/1.4954039, Available at http://scitation.aip.org/content/aip/journal/apl/108/25/10.1063/1.4954039

10. Horley, P. P., Jiménez, L. L., García, S. a P., Quintana, J. Á., Vorobiev, Y. V, Bon, R. R., Makhniy, V. P., and Hernández, J. G. "**Thin Film Solar Cells : Modeling , Obtaining and Applications**" *Intech* (2013):

11. Ohring, F. M. "**Materials Science of Thin Film: Deposition and Structure**" *Books* (2002): doi:10.1002/1521-3773(20010316)40:6<9823::AID-ANIE9823>3.3.CO;2-CAcademic Press

12. Krebs, F. C., Fyenbo, J., and Jørgensen, M. "**Product Integration of Compact Roll-to-Roll Processed Polymer Solar Cell Modules: Methods and Manufacture Using Flexographic Printing, Slot-Die Coating and Rotary Screen Printing**" *Journal of Materials Chemistry* 20, no. 41 (2010): 8994. doi:10.1039/c0jm01178a

13. Ahn, S. H. and Guo, L. J. "**High-Speed Roll-to-Roll Nanoimprint Lithography on Flexible Plastic Substrates**" *Advanced Materials* 20, no. 11 (2008): 2044–2049.

doi:10.1002/adma.200702650

14. Gamerith, S., Klug, A., Scheiber, H., Scherf, U., Moderegger, E., and List, E. J. W. "**Direct Ink-Jet Printing of Ag-Cu Nanoparticle and Ag-Precursor Based Electrodes for OFET Applications**" *Advanced Functional Materials* 17, no. 16 (2007): 3111–3118. doi:10.1002/adfm.200600762

15. Forrest, S. R. "**The Path to Ubiquitous and Low-Cost Organic Electronic Appliances on Plastic.**" *Nature* 428, no. 6986 (2004): 911–918. doi:10.1038/nature02498

16. Wagner, S. and Bauer, S. "**Materials for Stretchable Electronics**" *MRS Bulletin* 37, no. 3 (2012): 207–213. doi:10.1557/mrs.2012.37

17. Lacour, S. P., Wagner, S., Narayan, R. J., Li, T., and Suo, Z. I. "**Stiff Subcircuit Islands of Diamondlike Carbon for Stretchable Electronics**" *Journal of Applied Physics* 100, no. 1 (2006): 1–6. doi:10.1063/1.2210170

18. Lacour, S. P., Jones, J., Wagner, S., Li, T., and Suo, Z. "**Stretchable Interconnects for Elastic Electronic Surfaces**" *Proceedings of the IEEE* 93, no. 8 (2005): 1459–1466. doi:10.1109/JPROC.2005.851502

19. Gray, D. S., Tien, J., and Chen, C. S. "**High-Conductivity Elastomeric Electronics (Adv. Mater. 2004, 16, 393.)**" *Advanced Materials* 16, no. 6 (2004): 477–477. doi:10.1002/adma.200490017

20. Hsu, Y. Y., Gonzalez, M., Bossuyt, F., Vanfleteren, J., and Wolf, I. De. "**Polyimide-Enhanced Stretchable Interconnects: Design, Fabrication, and Characterization**" *Ieee Transactions on Electron Devices* 58, no. 8 (2011): 2680–2688. doi:Doi 10.1109/Ted.2011.2147789

21. Sun, Y., Choi, W. M., Jiang, H., Huang, Y. Y., and Rogers, J. a. "**Controlled Buckling of Semiconductor Nanoribbons for Stretchable Electronics.**" *Nature nanotechnology* 1, no. 3 (2006): 201–207. doi:10.1038/nnano.2006.131

22. Lacour, S. P., Tsay, C., and Wagner, S. "**An Elastically Stretchable TFT Circuit**" *IEEE Electron Device Letters* 25, no. 12 (2004): 792–794. doi:10.1109/LED.2004.839227

23. Watanabe, M., Shirai, H., and Hirai, T. "**Wrinkled Polypyrrole Electrode for Electroactive Polymer Actuators**" *Journal of Applied Physics* 92, no. 8 (2002): 4631–4637. doi:10.1063/1.1505674

24. Keplinger, C., Li, T., Baumgartner, R., Suo, Z., and Bauer, S. "**Harnessing Snap-through Instability in Soft Dielectrics to Achieve Giant Voltage-Triggered Deformation**" *Soft Matter* 8, no. 2 (2012): 285–288. doi:10.1039/C1SM06736B

25. Lacour, S. P., Chan, D., Wagner, S., Li, T., and Suo, Z. "**Mechanisms of Reversible Stretchability of Thin Metal Films on Elastomeric Substrates**" *Applied Physics Letters* 88, no. 20 (2006): 2004–2007. doi:10.1063/1.2201874

26. Woo, N. C., Cherenack, K., Tröster, G., and Spolenak, R. "**Designing Micro-Patterned Ti Films That Survive up to 10% Applied Tensile Strain**" *Applied Physics A: Materials Science and Processing* 100, no. 1 (2010): 281–285. doi:10.1007/s00339-010-5806-x

27. Glushko, O., Cordill, M. J., Klug, A., and List-Kratochvil, E. J. W. "**The Effect of Bending Loading Conditions on the Reliability of Inkjet Printed and Evaporated**

Silver Metallization on Polymer Substrates" *Microelectronics Reliability* 56, (2016): 109–113. doi:10.1016/j.microrel.2015.10.007, Available at http://dx.doi.org/10.1016/j.microrel.2015.10.007 Elsevier Ltd

28. Alzoubi, K., Hamasha, M. M., Schadt, M., Lu, S., Sammakia, B., and Poliks, M. "**Effect of Lamination on the Bending Fatigue Life of Copper Coated PET Substrate**" *Advances* 7956, (2011): 1–9. doi:10.1117/12.874226

29. Lee, H.-Y., Yi, S.-M., Lee, J.-H., Lee, H.-S., Hyun, S., and Joo, Y.-C. "**Effects of Bending Fatigue on the Electrical Resistance in Metallic Films on Flexible Substrates**" *Metals and Materials International* 16, no. 6 (2010): 947–951. doi:10.1007/s12540-010-1213-2, Available at http://link.springer.com/10.1007/s12540-010-1213-2

30. Glushko, O. and Cordill, M. J. "**Electrical Resistance of Metal Films on Polymer Substrates under Tension**" *Experimental Techniques* no. 1 (2014): 9–12. doi:10.1111/ext.12082

31. Jörg, T., Cordill, M. J., Franz, R., Glushko, O., Winkler, J., and Mitterer, C. "**The Electro-Mechanical Behavior of Sputter-Deposited Mo Thin Films on Flexible Substrates**" *Thin Solid Films* 606, (2016): 45–50. doi:10.1016/j.tsf.2016.03.032Elsevier B.V.

32. Xiang, Y., Li, T., Suo, Z., and Vlassak, J. J. "**High Ductility of a Metal Film Adherent on a Polymer Substrate**" *Applied Physics Letters* 87, no. 16 (2005): 1–3. doi:10.1063/1.2108110

33. Lacour, S. P., Wagner, S., Huang, Z., and Suo, Z. "**Stretchable Gold Conductors on Elastomeric Substrates**" *Applied Physics Letters* 82, no. 15 (2003): 2404–2406. doi:10.1063/1.1565683

34. Alzoubi, K., Lu, S., Sammakia, B., and Poliks, M. "**Factor Effect Study for the High Cyclic Bending Fatigue of Thin Films on PET Substrate for Flexible Displays Applications**" *IEEE/OSA Journal of Display Technology* 7, no. 6 (2011): 348–355. doi:10.1109/JDT.2010.2076772

35. Lu, N., Wang, X., Suo, Z., and Vlassak, J. "**Metal Films on Polymer Substrates Stretched beyond 50%**" *Applied Physics Letters* 91, no. 22 (2007): doi:10.1063/1.2817234

36. Glushko, O., Klug, A., List-Kratochvil, E. J. W., and Cordill, M. J. "**Relationship between Mechanical Damage and Electrical Degradation in Polymer-Supported Metal Films Subjected to Cyclic Loading**" *Materials Science and Engineering: A* 662, (2016): 157–161. doi:10.1016/j.msea.2016.03.052, Available at http://linkinghub.elsevier.com/retrieve/pii/S0921509316302556 Elsevier

37. Glushko, O. and Cordill, M. J. "**Electrical Resistance of Metal Films on Polymer Substrates**" *Experimental Techniques* 40, no. 1 (2016): 303–310. doi:10.1111/ext.12082

38. Yang, S., Su, B., Bitar, G., and Lu, N. "**Stretchability of Indium Tin Oxide (ITO) Serpentine Thin Films Supported by Kapton Substrates**" *International Journal of Fracture* 190, no. 1–2 (2014): 99–110. doi:10.1007/s10704-014-9977-x

39. Lu, N., Suo, Z., and Vlassak, J. J. "**The Effect of Film Thickness on the Failure Strain of Polymer-Supported Metal Films**" *Acta Materialia* 58, no. 5 (2010): 1679–1687. doi:10.1016/j.actamat.2009.11.010, Available at

http://dx.doi.org/10.1016/j.actamat.2009.11.010 Acta Materialia Inc.

40. Glushko, O. and Cordill, M. J. "**Electrical Resistance Decrease due to Grain Coarsening under Cyclic Deformation**" *Jom* 66, no. 4 (2014): 598–601. doi:10.1007/s11837-014-0943-x

41. Sim, G., Lee, Y., Lee, S., and Vlassak, J. J. "**Effects of Stretching and Cycling on the Fatigue Behavior of Polymer-Supported Ag Thin Films**" *Materials Science & Engineering A* 575, (2013): 86–93. doi:10.1016/j.msea.2013.03.043, Available at http://dx.doi.org/10.1016/j.msea.2013.03.043 Elsevier

42. Cordill, M. J., Glushko, O., Kreith, J., Marx, V. M., and Kirchlechner, C. "**Measuring Electro-Mechanical Properties of Thin Films on Polymer Substrates**" *Microelectronic Engineering* 137, (2014): 96–100. doi:10.1016/j.mee.2014.08.002, Available at http://linkinghub.elsevier.com/retrieve/pii/S0167931714003347 Elsevier B.V.

43. Marx, V. M., Toth, F., Wiesinger, A., Berger, J., Kirchlechner, C., Cordill, M. J., Fischer, F. D., Rammerstorfer, F. G., and Dehm, G. "**The Influence of a Brittle Cr Interlayer on the Deformation Behavior of Thin Cu Films on Flexible Substrates: Experiment and Model**" *Acta Materialia* 89, (2015): 278–289. doi:10.1016/j.actamat.2015.01.047, Available at http://dx.doi.org/10.1016/j.actamat.2015.01.047 Acta Materialia Inc.

44. Rickard, S. "**Characterization of Printed Planar Electromagnetic Coils Using Digital Extrusion and Roll-to-Roll Flexographic Processes**" (2015):

45. Putz, B., Volker, B., Semprimoschnig, C., and Cordill, M. J. "**Influence of Extreme Thermal Cycling on Metal-Polymer Interfaces**" *Microelectronic Engineering* 167, (2017): 17–22. doi:10.1016/j.mee.2016.10.012, Available at http://dx.doi.org/10.1016/j.mee.2016.10.012 Elsevier B.V.

46. Berger, J., Glushko, O., Marx, V. M., Kirchlechner, C., and Cordill, M. J. "**Effect of Microstructure on the Electro-Mechanical Behavior of Cu Films on Polyimide**" *Jom* 68, no. 6 (2016): 1640–1646. doi:10.1007/s11837-016-1940-z

47. Glushko, O., Marx, V. M., Kirchlechner, C., Zizak, I., and Cordill, M. J. "**Recovery of Electrical Resistance in Copper Films on Polyethylene Terephthalate Subjected to a Tensile Strain**" *Thin Solid Films* 552, (2014): 141–145. doi:10.1016/j.tsf.2013.12.055, Available at http://dx.doi.org/10.1016/j.tsf.2013.12.055 Elsevier B.V.

48. Hutchinson, J. . and Suo, Z. "**Mixed Mode Cracking in Layered Materials**" *Advances in Applied Mechanics* 29, (1991): 63–191.

49. Cordill, M. J., Glushko, O., and Putz, B. "**Electro-Mechanical Testing of Conductive Materials Used in Flexible Electronics**" *Frontiers in Materials* 3, no. February (2016): 1–11. doi:10.3389/fmats.2016.00011, Available at http://journal.frontiersin.org/article/10.3389/fmats.2016.00011%5Cnhttp://journal.frontiersin.org/Article/10.3389/fmats.2016.00011/abstract

50. Kleinbichler, A., Bartosik, M., Völker, B., and Cordill, M. J. "**Thin Film Adhesion of Flexible Electronics Influenced by Interlayers**" *Advanced Engineering Materials* (2017): 1–7. doi:10.1002/adem.201600665

51. Glushko, O., Klug, A., List-Kratochvil, E. J. W., and Cordill, M. J. "**Monotonic and Cyclic Mechanical Reliabiltiy of Metallization Lines on Polymer Substrates**" *Journal*

of Materials Research under revi, (2017):

52. Kim, B.-J., Haas, T., Friederich, A., Lee, J.-H., Nam, D.-H., Binder, J. R., Bauer, W., Choi, I.-S., Joo, Y.-C., Gruber, P. a., and Kraft, O. "**Improving Mechanical Fatigue Resistance by Optimizing the Nanoporous Structure of Inkjet-Printed Ag Electrodes for Flexible Devices.**" *Nanotechnology* 25, no. 12 (2014): 125706. doi:10.1088/0957-4484/25/12/125706, Available at http://www.ncbi.nlm.nih.gov/pubmed/24577219